THE ANNUAL REPORT OF THE MSU GROUP
(Jan.-Dec. 2004)

Contributors: V.B.Braginsky (P.I.), I.A.Bilenko,.Ya.Khalili,
V.P.Mitrofanov, A.V.Stepanov, K.V.Tokmakov, S.P.Vyatchanin.
The researches were supported by NSF grant
"Low noise suspensions and readout systems for LIGO"
(PHY-0098715 July 2001—June 2004)
(PHY-0353775 July 2004 – June 2007)

Contents

Summary **2**

1 Experimental researches 2

1.1 The investigation of thermal and excess noise in the high-Q modes of all fused silica suspension for the Advanced LIGO test masses. . 2

1.2 The investigation of thermal and excess noise in the fused silica plates with multilayer reflective coating. 3

1.3 The investigation of effects associated with electrical charging of fused silica test masses 3

1.4 Nonstationary electrical charge distribution on the fused silica bifilar pendulum and its effect on the mechanical Q-factor 4

2 Theoretical researches 5

2.1 Corner reflectors in the main Fabry-Perot cavities 5

2.2 Double mirror test mass 6

3 Collaboration between MSU group and LIGO Lab, LSC and K.S.Thorne's group 7

4 Publication of MSU group members in 2004 9

5 Publication of MSU group members in collaborations with LIGO Lab and LSC in 2004 9

Appendixes **10**

A The investigation of thermal and non-thermal noises in Advanced LIGO suspension prototype. **11**

B Nonstationary electrical charge distribution on the fused silica bifilar pendulum and its effect on the mechanical Q **23**

C Corner reflectors and Quantum-Non-Demolition Measurements in gravitational wave antennae **29**

D Reducing the mirrors coating noise in laser gravitational-wave antennae by means of double mirrors **54**

Summary

1 Experimental researches

1.1 The investigation of thermal and excess noise in the high-Q modes of all fused silica suspension for the Advanced LIGO test masses.

The program of these investigations was formulated several years ago after the discovery made by MSU group of the excess noise in steel wires [1]. During previous years (2000-2003) new technique of measurements of Brownian and excess noise in fused silica fibers used in the suspension was proposed and realized by I.A.Bilenko and his students. This technique allowed to monitor the vibrations of thin fused silica fibers with sensitivity $S_x = 3 \times 10^{-13}\,\mathrm{cm}/\sqrt{\mathrm{Hz}}$ near the frequency 1 kHz and $S_x < 9 \times 10^{-14}\,\mathrm{cm}/\sqrt{\mathrm{Hz}}$ at frequencies higher than 2 kHz (these values even slightly exceed requirements declared in the grant proposal). With this sensitivity it is possible to resolve the energy innovation on chosen mode during the time interval $t = 0.1\,\mathrm{c}$ that corresponds to $\simeq 1\%$ of kT. The analysis shows, that the future improvement isn't possible unless the principal and costly modifications will be made. No any significant excess noise for 10 different samples tested under stress varies from 3% to 15% of breaking value was observed.

During the January-June of the 2004 I.A.Bilenko concentrated his efforts on the measurements on the samples under higher stress. Finally, 4 series of records on the samples under stress $> 40\%$ from breaking value was obtained.

During the June-December of the 2004 all the obtained data was evaluated using the universal algorithm. Part of the records was excluded from the investigation due to insufficient sensitivity of the readout system at the time of the records.

Total duration of the refined records is about 90 hours obtained on 9 fused silica samples loaded from $\approx 4\%$ to $\approx 50\%$ of breaking stress. At the level limited by the sensitivity of our apparatus only Brownian noise was registered. This result may be regarded as a part of approval of the Advanced LIGO suspension design. Complete report on the excess noise program is in the Appendix A. The final paper about the retrieval of the excess noise in the stressed fibers will be submitted to Physics Letters after the LIGO approval.

1.2 The investigation of thermal and excess noise in the fused silica plates with multilayer reflective coating.

A new program of experimental researches was stimulated by the analysis of the contribution of the thermoelastic noise in the coating into the total noise budget performed by V.B.Braginsky and S.P.Vyatchanin in 2003 [2] as well as the consequent direct measurements of the thermal expansion coefficient $\alpha_{Ta_2O_5}$ performed by A.A.Samoilenko [3]. These analysis and measurements have shown that thermoelastic noise may prevent to reach the sensitivity of the Advanced LIGO antenna better than SQL. On the other hand the method used for the $\alpha_{Ta_2O_5}$ measurement based on the bending of thin SiO_2 plates under heating demonstrated that the sum of Brownian, thermoelastic and, probably, excess noise components would be not too difficult to register. This approach looks promising because in essence it will be an examination of the "behaviour" of thermal and nonthermal fluctuations in the reflective coating identical to the coatings which will be used in Advanced LIGO.

I.A.Bilenko and A.V.Stepanov started the implementation of this experimental program.

At present a new vacuum chamber for this program is prepared and tested as well as antiseismic isolation for the optical mini-table.

The shadow sensor based on the He-Ne laser was prepared for preliminary measurement of the quality factor of the thin fused silica plates coated with reflecting multilayer. We also prepared components for the optical sensor based on Fabry-Perot cavity pumped by stabilized Nd:YAG laser. The projected sensitivity is $\simeq 5 \times 10^{-14}\mathrm{cm}/\sqrt{\mathrm{Hz}}$ at 500 Hz. The Pound-Drever scheme and other optic parts are under development now.

1.3 The investigation of effects associated with electrical charging of fused silica test masses

V.P. Mitrofanov, K.V. Tokmakov and postgraduate student L.G. Prokhorov in the collaboration with Phil Willems (Caltech) in 2004 continued the investigation of effects associated with charging of fused silica test mass. During 2003, in first version of the set up the vertically oriented plate with capacitive probe electrodes connected to high impedance amplifier was placed in parallel with the end face of suspended fused silica cylinder so that the separation gap was of about 3 mm. The initial amplitude of torsion oscillations of the cilinder was about 2 mm. Nevertheless pendulum could swing far enough to be very close to the plate with electrodes due to the local seismic exitation.

During January – June 2004 V.P. Mitrofanov and his colleagues carried out the search of variation of the charge located on the cylinder when the provoked touching of the plate with electrodes by the cylinder took place. It was found that the provoked touching resulted in the jump-like changes of the pendulum amplitude and the probe signal (which was proportional to the electrical charge on the cylinder) analogously to the events observed in 2003. But there was at least two distinctions in the behaviour of the system "pendulum-electrodes" in case of the provoked touching: 1) changes of the amplitude and the probe signal were faster than in case of events observed earlier; 2) admission of a small portion of air into vacuum chamber resulted in the significant drop of the probe signal, whereas after events the probe signal could be reduced only by electrical discharge in poor vacuum. (See details in [4] and [5]).

1.4 Nonstationary electrical charge distribution on the fused silica bifilar pendulum and its effect on the mechanical Q-factor

V.P.Mitrofanov, K.V.Tokmakov and postgraduate student L.G.Prokhorov continued the investigation of effects associated with charging of the fused silica test mass. In the previous measurements which were carried out in MSU and the other groups the electrical charge located on the test mass was in the state close to the stationary state. This year the MSU group began to study the dissipation in the case when the electrical charge was in nonstationary one. A number of new experimental data was obtained.

The behavior of electrical charges located on a 0.5 kg fused silica cylinder suspended on two fused silica fibers in vacuum of about 10^{-7} Torr was investigated. Several modifications of the previous version of the set up were done. The fused silica plate with gold electrodes deposited on it being horizontally oriented was placed under the cylinder with the separation gap of about 1 mm. These electrodes were the nearest objects electrical charges could interact with. The charge located on the cylinder was measured by means of the capacitive probe. This probe (2 cm^2 copper plate connected with the electrometric amplifier) was placed at the side of the cylinder at a distance of 2 cm so that it monitored some effective electrical charge located on the cylinder.

The average value of charge density on the fused silica cylinder was of the order of 10^{-12} C/cm^2 (*i.e.* 10^7 electrons/cm^2). In this case the Q of the bifilar torsion mode was about 6×10^7. This value of Q was lower than those obtained for the pendulum when nothing was close enough to the suspended cylinder ($Q \gtrsim 9 \times 10^7$). So it is possible to suppose that the reduction of the pendulum Q was associated with electrical charges located on the fused silica cylinder and their interaction with the electrodes under the pendulum.

The disturbance in the distribution of electrical charges on the pendulum was produced by two ways. The first one was realized by means of touching the fused silica cylinder by a metal wire. A special manipulator was used. The local deposition of the charge occurred in the point of touching (1.5 cm below of the center of the cylinder) due to the contact electrification. After this the deposited charge spread over the cylinder due to diffusion. Another way to disturb the charge distribution was to create electric field applying high voltage to the electrodes, which were under the pendulum. After the voltage 1400 V was switched on during 24 hours one could observe the relaxation of the voltage from the probe as well as in the first case. After the transient in the first several hours the decay of the voltage with the relaxation time of the order of 200 hours was recorded in both cases.

After the disturbances of the charge distribution it was observed that the behavior of the pendulum amplitude free decay had some feature. In the first case the rate of the free decay of the pendulum amplitude remained invariable in limits of the uncertainty of the measurements associated mainly with the seismic noise. In the second case after the voltage was switched off the rate of the free decay of the pendulum amplitude during approximately 200 hours was lower than before the application of the high voltage. This change in the rate was too large and lasted too long to be associated with seismic fluctuations. After that the rate of the decay returned back to the initial value. Such behavior can be interpreted as if it was associated with the increase of the pendulum Q from about 6×10^7 up to $(1 \div 2) \times 10^8$. The uncertainty in the last value was caused by the uncertainty of the approximation of the pendulum amplitude time dependence in

this range. Within these limits the rate of the amplitude decrease was different in various runs of measurements.

After the contact electrification the relaxation of the charge distribution was observed but the change of the pendulum Q was not detected. This can be explained by the large distance between the point of the contact and the electrodes. Four runs of the measurements were carried out. Every run had duration from 600 hours to 1600 hours. The behaviors of the free decay of the amplitude described above were observed in every run. The transient observed in the first several hours after the disturbances of the charge distribution needs more detailed investigation. The measurements are in progress. It is necessary to find the dependence of these effects on duration of the high voltage application and on the other factors. The aim of the research is to identify the mechanism of losses and noise associated with charging of the test masses (see details in Appendix B).

Also V. P. Mitrofanov and his colleagues began to test the new setup for the search of the spatial charge distribution over the surface of fused silica samples and other dielectric materials which might be used in the test masses. The setup has a good potential sensitivity but a number of parasitic effects need to be eliminated.

2 Theoretical researches

It was emphasized in section 1.2 of this report that theoretical analysis and direct measurements performed by the members of MSU group have shown that thermoelastic noise in multi-layer dielectrical coating of the mirrors initially planned in advanced LIGO project will not permit to reach the sensitivity substantially better than standard quantum limit (SQL) (see publications [2, 3] and MSU group 2003 annual report). This motivated not only the start of a new experimental program described in section 1.2, but also the searches of new types of reflective mirrors. Two types of such new mirrors were proposed and analyzed. The net result of these analysis shows that using any of two proposed types it is possible to circumvent SQL sensitivity with a factor about ten if thermoelastic noise is the only limiting factor.

2.1 Corner reflectors in the main Fabry-Perot cavities

The key idea of this version proposed by V. B. Braginsky and S. P. Vyatchanin is based on the concept of corner reflectors (CR) — tri-hedral or two-hedral prisms. These CR may play the role of high finesse reflectors instead of cylindrical shape mirrors with multi-layer dielectric coating. To make stable the chosen optical mode it is necessary to make the "foot" of such a CR with finite value of curvature. To evade the reflection of the light from the "foot" (and thus to exclude the creation of additional set of optical modes in the cavity) it is necessary to cover the "foot" with relatively small number (2-4 pairs) of anti-reflective layers. Taking into account that usual reflective coating has 20 - 40 pairs of layers, it is reasonable to expect that with such a thin anti-reflective coating the thermoelastic noise in it will be about one order smaller.

Pure fused silica (SiO_2) is an appropriate glass to manufacture corner reflectors because its refractive index $n_{\mathrm{SiO_2}} = 1.45$. This value is sufficiently large to provide total internal reflection (due to Snellius law) both for two or three facets CR: $n_{\mathrm{SiO_2}} > \sqrt{2}$ (two facets) and $n_{\mathrm{SiO_2}} > \sqrt{3/2}$ (three facets). V. B. Braginsky and S. P. Vyatchanin have

carried out in depth analysis for the conditions which have to be fulfilled to implement CR:

1. the conditions for the displacements of one CR relatively to the second CR;
2. the conditions for the tilt angle of one CR;
3. the conditions for the exposure angle (angle between facets);
4. the fundamental difractional losses on the edge where two facets meet.

The analysis shows that today existing technology of mechanical manufacturing and positioning allow to satisfy these conditions.

The only "fee" which has to be paid for such a version of Fabry-Perot cavity is the necessity to use non-Gaussian distribution of the light over cross section of beam — so called mesa-beams [6, 7]. The origin of this "fee" is thermo-refractive noise in the bulk of CR (this noise originates from thermodynamic temperature fluctuations which produced the phase fluctuations in reflected wave due to dependence of refractive index on temperature).

There is also one potential possibility to evade the usage of CR: to find such a glass for multi-layer coating which has the value of thermo-refractive index close to the value $n_{\mathrm{Ta_2O_5}} \simeq 2.1$ but with thermal expansion factor close to the value of fused silica thermal expansion.

See details in Appendix C and in [8].

2.2 Double mirror test mass

An alternative concept of a Fabry-Perot cavity with substantially reduced thermoelastic noise in the mirrors coating was proposed by F.Ya.Khalili.

Key idea of this elegant concept is to use two independently suspended mirrors separated by relatively small distance $l = 30 - 1000\,\mathrm{cm}$ instead of a single high-reflective mirror in the end of the Fabry-Perot cavity. These mirrors may have the same cylindrical shape and masses as it is planned in Advanced LIGO. The mirrors "working" surfaces have to be parallel to each other.

In this double mirror test mass the first surface which "meet" the incident beam has to have relatively small reflectivity, *e.g.* $1 - \mathcal{R}_1 \sim 10^{-2}$. The second surface of the first mirror has to have thin antireflective coating. The third surface (the first of the second mirror) has to have high reflectivity, *e.g.* $1 - \mathcal{R}_2 \approx 10^{-5}$. With these numerical values, the total reflectivity of such a double mirror will be defined by the following relation:

$$1 - \mathcal{R} \approx \frac{(1 - \mathcal{R}_1)(1 - \mathcal{R}_2 + 2\mathcal{A})}{4} \lesssim 10^{-7}\,, \tag{.1}$$

if the first mirror absorption $\mathcal{A} \approx 10^{-5}$ and the optical distance between the mirrors' reflective surfaces

$$l = \left(N + \frac{1}{4}\right)\lambda \tag{.2}$$

(*i.e* the anti-resonance condition, λ is the wavelength and N is an integer). It have to be emphasized, that in this example only about 0.25% of the light power will circulate between the two mirrors.

Thermoelastic noise in the coating in this double mirrors system will be substantially reduced because the main contribution may be from the first surface of the first mirror (which reflects most of the light power), but this surface is about $3 \div 5$ times thinner than it is planned for the Advanced LIGO ETM mirrors, and correspondingly the contribution of the thermoelastic noise in this surface to the total noise budget will be reduced with the same factor.

The remaining small fraction of the light power will be reflected from the second mirror. This fraction of the power will be substantially "contaminated" by the thermoelastic noise in the coating of the second mirror (which will have thick multilayers reflector). However, its part is the sum noise from two mirrors will be negligible small in comparison with the part of the first mirror.

This new concept has another advantage: the mass of the second mirror may be substantially smaller than the mass of the first one (in the above numerical example it may be 10^6 times smaller). This reduction of the second mass will not increase the value of the SQL.

See details in Appendix D and in [9].

3 Collaboration between MSU group and LIGO Lab, LSC and K.S.Thorne's group

Members of the MSU group have visited Caltech for research collaboration and extensive discussions: V.B.Braginsky — two times, V.P.Mitrofanov, S.P.Vyatchanin and F.Ya.Khalili — once.

V.P.Mitrofanov has given a talk at the LSC meeting at Livingston Observatory; S.P.Vyatchanin and F.Ya.Khalili — at the LSC meetng at Hanford observatory.

V.P.Mitrofanov have visited University of Glasgow. He gave a talk at the seminar and took part in experimental work in the laboratory and had fruitful discussions with members of Glasgow group about various mechanisms of dissipation in the test masses of LIGO project.

The members of MSU group in the collaboration with P.Willems (LIGO, Caltech) continued long lasting measurements of variations of electrical charge located on the fused silica test mass prototype and searched for correlations between these variations and cosmic ray shower events.

The total number of seminars and presentations by V.B.Braginsky, V.P.Mitrofanov, S.P.Vyatchanin, and F.Ya.Khalili is 3 at Caltech and is 3 at LSC meetings.

References

[1] I.A.Bilenko, A.Yu.Ageev, V.B.Braginsky , Physics Letters A **246**, 479 (1998).

[2] V.B.Braginsky, S.P.Vyatchanin, Physics Letters A **312**, 169 (2003).

[3] V.B.Braginsky, A.A. Samoilenko, Physics Letters A **315**, 175 (2003).

[4] V.Mitrofanov, L.Prokhorov, K.Tokmakov and P.Willems, Class. Quantum Grav. **21**, 1083 (2004).

[5] V.Mitrofanov, L.Prokhorov, K.Tokmakov and P.Willems, Talk at LSC meeting, Louisiana, March 15-18, (2004).

[6] E. d'Ambrosio, R. O'Shaughnessy, S. Strigin, K.Thorne and S. Vyatchanin, Reducing Thermoelastic Noise in Gravitational-Wave Interferometers by Flattening the Light Beams, submitted to *Phys. Rev. D*,
available as file beamreshape020903.pdf at http://www.cco.caltech.edu/∼kip/ftp/

[7] O'Shaughnessy, S. Strigin and S. Vyatchanin, The implifications of Mexican-hat mirrors: calculations of thetmoelastic noise and interferometer sensitivity to perturbation for Mexican-hat mirror proposal for advanced LIGO, submitted to *Phys. Rev. D.*

[8] V.B.Braginsky, S.P.Vyatchanin, Physics Letters A **324**, 345 (2004).

[9] F.Ya.Khalili, arXiv:gr-qc/0406071 (2004).

4 Publication of MSU group members in 2004

1. B. B. Braginsky and S. P. Vyatchanin,
"Corner reflectors and quantum-non-demolition measurements in gravitational wave antennae",
Physics Letters **A324** (2004) 345-360, arXiv:cond-mat/0402650.

2. I. A. Bilenko, V. V. Braginsky, S. L. Lourie,
"Mechanical losses in thin fused silica fibers",
Class. Quantum Gravity, **21** (2004) 1231.

3. M. L. Gorodetsky, I. S. Grudinin,
"Fundamental thermal fluctuations in microspheres",
Journal of Optical Siciety of America **B21** (2004) 697.

4. F.Ya.Khalili, "Reducing the mirrors coating noise in laser gravitational-wave antennae by means of double mirrors", *accepted for publication in Physics Letters A*, arXiv:gr-qc/0406071.

5. V.Mitrofanov, L.Prokhorov, K.Tokmakov and P.Willems, "Investigation of effects associated with variation of electric charge on a fused silica test mass", Class. Quantum Grav. **21**, 1083 (2004).

5 Publication of MSU group members in collaborations with LIGO Lab and LSC in 2004

1. B. Abbott et al. (LSC including I. A. Bilenko, V. B. Braginsky, V. P. Mitrofanov, S.P. Vyatchanin) "Detector Description and Performance for the First Coincidence Observations Between LIGO and GEO" *Nuclear Instrum and Methods in Physics Research"* **A517** (2004) 145.

2. B. Abbott et al. (LSC including I. A. Bilenko, V. B. Braginsky, V. P. Mitrofanov, S.P. Vyatchanin), "First Upper Limits from LIGO on GW Bursts", *Phys. Rev.* **D69** (2004) 102001.

3. B. Abbott et al. (LSC including I. A. Bilenko, V. B. Braginsky, V. P. Mitrofanov, S.P. Vyatchanin), "Setting Upper Limits on the Strength of Periodic GW from PSR J1939 + 2134 Using the First Science Data from the GEO600 and LIGO Detectors", *Phys. Rev.* **D69** (2004) 082004.

4. B. Abbott et al. (LSC including I. A. Bilenko, V. B. Braginsky, V. P. Mitrofanov, S.P. Vyatchanin), "Analysis of LIGO Data for GW from Binary Neutron Stars", *Phys. Rev.* **D69** (2004) 122001.

5. B. Abbott et al. (LSC including I. A. Bilenko, V. B. Braginsky, V. P. Mitrofanov, S.P. Vyatchanin), "Analysis of LIGO Data for Stochastic GW", *Phys. Rev.* **D69** (2004) 122004.

Appendixes

Appendix A

The investigation of thermal and non-thermal noises in Advanced LIGO suspension prototype.

The results of experimental investigation of the mechanical noise produced by fused silica fibers is reported. The best achieved resolution is about $0.01\,kT$ for the modes with quality factor from 10^5 to 10^7. Over the 90 hours of observation no excess (additional to Brownian) noise was found in fibers loaded at $4\% \div 50\%$ from breaking stress.

Introduction

The planned sensitivity in the second generation of the Laser Interferometer Gravitational wave Observatory (Advanced LIGO) has to be close to the value of the amplitude of the perturbation of metric $h \simeq 10^{-22}$ (from the frequency 100 Hz to 1 kHz and in the bandwidth about 100 Hz) [1]. This value of h corresponds to the amplitude of oscillation of antenna's mirror relatively another one about $\Delta x_{gr} \simeq 2 \times 10^{-17}$ cm.These values of h and Δx_{gr} are approximately ten times smaller than the recently achieved sensitively in one of the two operating LIGO antennae (Initial LIGO), see [2]. The planned gain in the sensitivity means that all kinds of noises in the antennae have to be correspondingly reduced.

Starting from 1991 several groups of researchers in LIGO Scientific Collaboration (LSC) and several researches from LIGO Lab were steady searching new types of material for the mirrors and new types of mirror's suspensions which allow to increase substantially the mechanical quality factors Q in all modes of mirror itself and mirrors suspension. The Fluctuation-Dissipation Theorem (FDT) predicts that to obtain a gain of one order in sensitivity it is necessary to increase the values of Q by two orders.

Several groups of researches which belong to LSC and LIGO Lab obtained very promising value of Q factors in the models of mirrors and in the suspension modes using extremely pure fused silica. The Q of pendulum mode and violin modes of such suspension turned out to exceed 10^8 at room temperature [3]-[7]. These values are approximately three orders higher than the Q in pendulum and violin modes in the steel wires suspension which are used at present in Initial LIGO [8]. Thus, "from the point of view of FDT" it is reasonable to expect at least one order of gain in the sensitivity. But FDT may predict the values of thermal noise in thermal equilibrium only, not the so-called excess noise (of

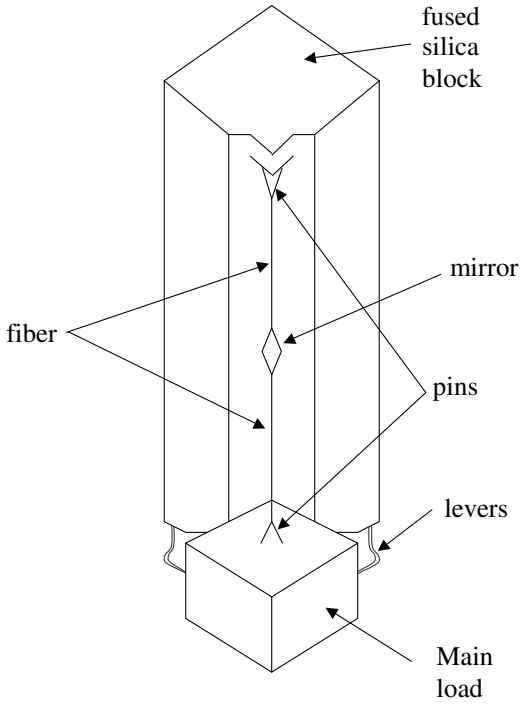

Figure A.1: Samples support design

non-thermal origin). This noise (or noises) particulary appears due to the transformations of free energy accumulated in solids from the static elastic form (typical free energy in solid is about 10^6 erg/g) to the kinetic (oscillatory) one. The probability of these transformations ("leakages") increases when the mechanical stress is applied. Such an effect was observed in steel wires which are used in the Initial LIGO suspension. Noise bursts were observed in some well stressed samples [9].

If, as planned, the violin mode's quality factor of Advanced LIGO suspension fibers will be $Q_{viol} \simeq 10^8$, then, according to FDT, the rms variation of energy stored in this mode over a half of period has to be $\delta E \simeq 2kTQ_{viol}^{-1/2} \simeq 4\times10^{-18}$ erg at room temperature. This value is 10^{21} times (!) smaller than the total free energy stored in one milligram fiber. Thus even very small "leakage" of free energy into violin mode may effectively "warm" it and degrade the antenna sensitivity.

The above arguments motivated investigations described in this article in which author's goal was to measure the noises in high Q modes of fused silica suspension prototype resolving small fraction of kT - mean energy of thermal equilibrium oscillations.

Experimental setup

To achieve the sensitivity mentioned above on the fused silica fiber suspension prototype the installation used in [9] was substantially redesigned. One of the key elements of the installation was heavy fused silica block (see Figure A.1) with a rigid horizontal cantilever with a pin carved from it. Upper end of the fibers were welded to this pin. The lower end

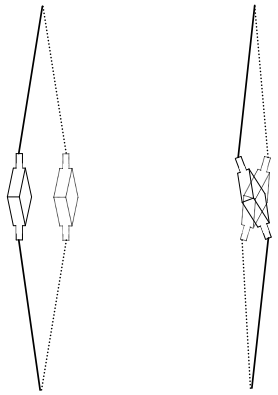

Figure A.2: Violin-like (left) and mirror-swinging (right) modes of the sample.

of the fiber were welded to a pin on a fused silica piece (main load, about 200 g). This piece was connected to the block by two thin horizontal levers. The stretching rigidity of the levers was high enough to prevent pendulum oscillations of the samples while bending one was small as compared to the longitudinal rigidity of the fibers.

Nearby the block there was an electrically driven manipulator which allowed to place a makeweight (additional load) automatically and observe the noise right after it.

The diameter of tested fibers was from $50\,\mu m$ to $180\,\mu m$, total length was 9.2 cm.

Another key element of the installation was an optical sensor based on a Fabry-Perot cavity. We have developed a technique of welding a small (approx. $4 \times 2 \times 0.5$ mm) diamond shaped mirror with high reflective multilyer coating on it which allows to keep the quite high quality factor of the violin-like mode (oscillation of the fiber with the lumped mass in the middle; in our case the masses of fibers were smaller then of the mirror). We also monitor a mirror-swinging mode of the mirror (see figure A.2) which has a quality factor $> 10^7$.

The Fabry-Perot cavity was formed by fixed spherical mirror (front) and mirror welded into the sample (end). Length of the cavity was 1.2 cm. The reflection coefficient of mirrors was $R = 0.97$, measured finesse varies from 50 to 100 for different samples.

The schematic diagram of the installation is shown on figure A.3. A He-Ne single frequency 2 mW stabilized laser (Mellies-Grot STP-903) has been used as a pump source. The light was passed through the pair of Faradey isolators, electro-optic modulator (EOM), beam splitter to the single mode waveguide input. Fraction of the light was used by amplitude noise suppression feedback chain (inclusive photodetector, amplifier and EOM) and also by the amplitude spikes monitor (see below). By the waveguide the light was passed inside the vacuum chamber, where, through the mode matching lens, illuminated the cavity. Behind the end mirror of the cavity a detector connected to twin low noise preamplifier was placed. Outputs of the preamplifier were connected to the pair of lock-in amplifiers (Stanford research SR810) pre-tuned to the selected modes frequencies and drift compensation feedback chain (inclusive band pass filters, amplifier and PZT drive attached to the front mirror mount). This chain allows to adjust the interferometer so the pump frequency was tuned to the slope of resonance curve. At this regime power

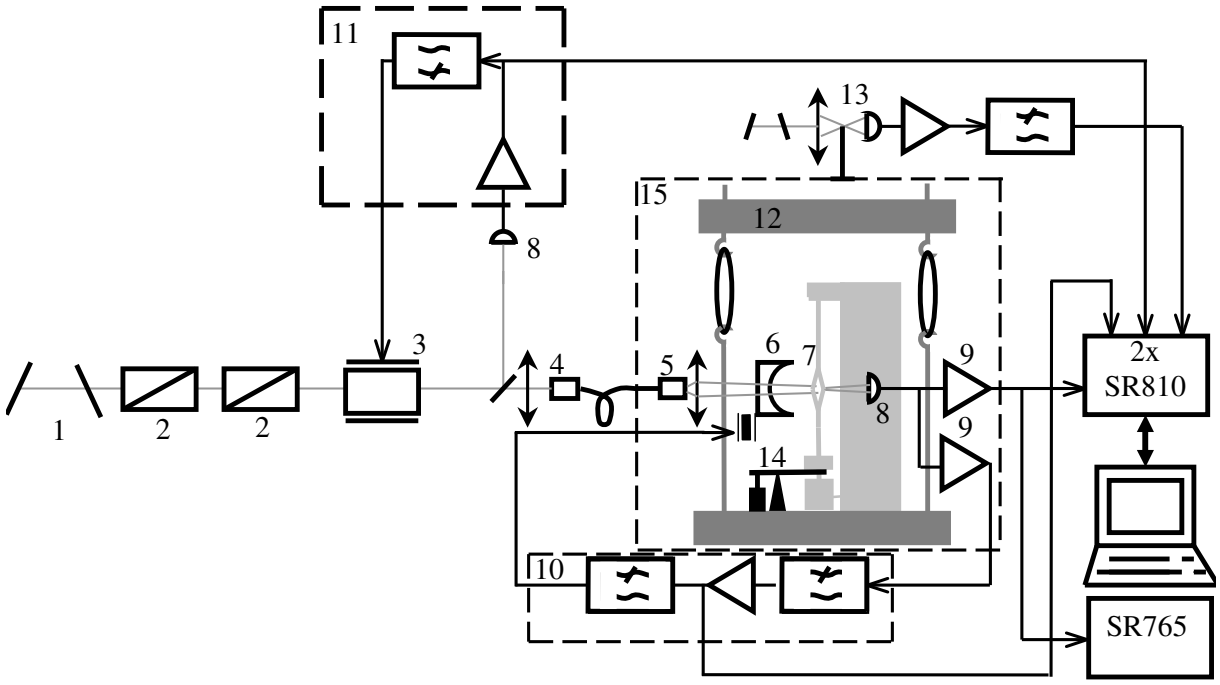

Figure A.3: The installation schematic diagram: 1-laser; 2-Faradey isolators; 3-EO modulator ; 4-wave guide launch ; 5-mode matching lens; 6-front mirror; 7-sample with the mirror welded; 8-photodetectors; 9-preamplifiers; 10-drift compensation feedback; 11-amplitude noise suppression feedback;12-anti-seismic suspension; 13-seismic shadow sensor; 14-makeweight manipulator; 15-vacuum chamber.

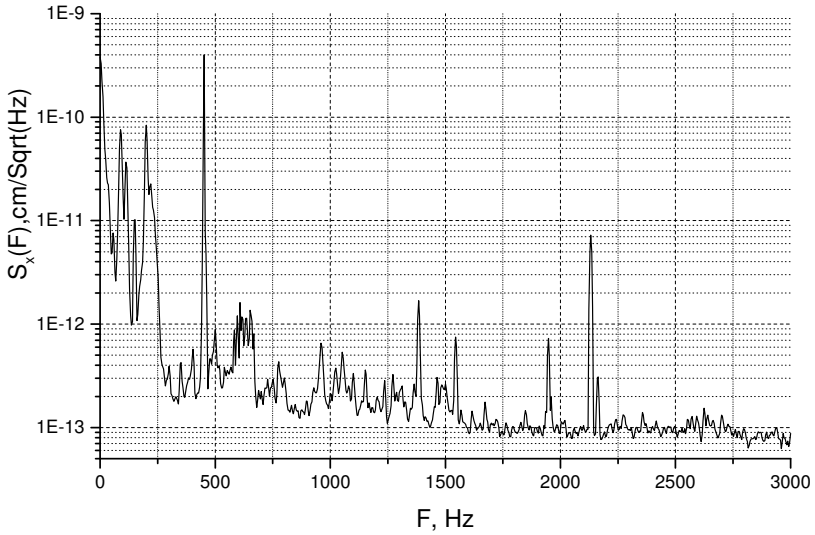

Figure A.4: Typical mirror oscillation spectrum. Spectrum analyzer binwidth was 4 Hz. Peaks at 450 Hz and 2130 Hz corresponds to violin-like and mirror-swinging modes, respectively.

collected by the detector was $\simeq 100\,\mu W$. For the finesse of the cavity $F = 100$ and quantum effectiveness of the detector $q = 0.5$ the ultimate sensitivity was:

$$S_x^{min} \simeq \frac{\lambda}{2F}\sqrt{\frac{\hbar\omega}{qW}} = 2.5 \times 10^{-14}\,\frac{cm}{\sqrt{Hz}} \tag{A.1}$$

The lowest noise floor achieved in the experiments corresponds to $S_x \simeq 9 \times 10^{-14}\,\frac{cm}{\sqrt{Hz}}$ which is 3 times higher than this shot noise limit (see figure A.4). We consider that the main contribution in this value and in the rise of the noise spectrum density in the $0.5-1.5$ kHz band mainly is from the residual laser phase noise. A new anti-seismic multistage suspension allowed to reduce noises induced by the environment vibrations. It consists of heavy (10 kg) brass disks suspended on gaunt viton rings (frequencies of stretching modes - 2.2 Hz, rocking mode 1.2 Hz).

In this installation we pay special attention to any possible external effects which may stimulate or mimic the excess noise in the tested fibers. In order to veto such an events we monitor microseismic near the vacuum chamber using a laser shadow sensor, pump laser power and the signal in the drift compensation feedback. The subsidiary ADC's of the SR810 have been used.

All signals (amplitudes of two selected modes and outputs of 3 monitor channels) were sampled at 100 1/s rate and passed to PC via IEEE488 bus.

Measurements and results

We presented results obtained on 9 fused silica samples loaded from $\approx 4\%$ to $\approx 50\%$ of breaking stress. The frequencies of oscillation on the violin-like mode ω_v were from 400

Hz to 750 Hz for different samples and its amplitudes corresponded to Brownian noise within $\approx 30\%$ accuracy (for the calibration we used a harmonic signal applied to the PZT drive):

$$\bar{A} = \sqrt{\frac{2kT}{m\omega_v^2}} = \sqrt{\frac{2 \times 4 \times 10^{-14}\, erg}{1 \times 10^{-2}\, g\, (2\pi \times 500\, Hz)^2}} \simeq 1 \times 10^{-9}\, cm \tag{A.2}$$

here $m \simeq m_m + 0.5\, m_f$, m_m is a mass of the the welded mirror, m_f - mass of the fiber.

This outcome confirms our previous results [10]. Short time variations were in a good agreement with [11]:

$$\bar{A_t^2} \simeq \bar{A}^2\, \frac{2t}{\tau^*} \tag{A.3}$$

here τ^* is a relaxation time for this mode. We choose the value of measurement (averaging) time $t = 0.1$ s.

It was difficult to make the same comparison accurate for the mirror-swinging mode, because of strong dependence of sensor conversion coefficient on the position of the reflection point on the mirror with respect to the rotation axes. Hence, an bearable assumption that the average amplitude measured for this mode also corresponds to the thermal motion wasn't checked. Nevertheless we processed all data for this mode on the same way as for violin-like one looking for non-Gaussian addition to the Gaussian distribution of the amplitude.

Test set Nr.	Sample code	Diameter and applied load(% of breaking stress for this sample)	Mode freq. $[Hz]$ and type	Quality factor	Obs. time (sec)	Noise floor	Nr. of candidate events	Nr. of excess events proved
1	Q2	$180\,\mu m, 4\%$	1087m	2×10^6	17000	5×10^{-2}	62	0
2	Q4	$120\,\mu m, 8\%$	762v	3.4×10^6	7450	1.5×10^{-2}	7	0
3			2319m	1×10^7	31300	4×10^{-2}	48	0
4	Q5	$90\,\mu m, 15\%$	1538m	7.4×10^6	14400	4×10^{-2}	26	0
5	Q6	$70\,\mu m, 19\%$	1932m	2×10^7	23600	1×10^{-2}	0	0
6	Q9	$85\,\mu m, 16\%$	748v	1.4×10^6	6700	3×10^{-2}	17	0
7			1980m	1×10^7	5050	5×10^{-2}	1	0
8	Q9	$85\,\mu m, 19\%$	759v	1.9×10^6				
			2197m	1.3×10^7	33450	5×10^{-2}	0	0
9	Q11	$70\,\mu m, 24\%$	1600m	1.4×10^7	16750	2×10^{-2}	0	0
10	Q11	$70\,\mu m, 29\%$	1747m	1.3×10^7	18250	2×10^{-2}	0	0
11	Q11	$70\,\mu m, 35\%$	1946m	9×10^6	16500	3×10^{-2}	0	0
12	Q11	$70\,\mu m, 42\%$	2083m	5×10^6	15850	6×10^{-2}	0	0
13	Q20	$75\,\mu m, 20\%$	624v	8.2×10^5	2400	3×10^{-2}	2	0
			1852m	8.5×10^6	2400	5×10^{-2}	0	0
14*	Q20	$75\,\mu m, 21\%$	627v	8.0×10^5	4800	3×10^{-2}	5	0
			1861m	8.5×10^6	4800	5×10^{-2}	0	0
15	Q21	$60\,\mu m, 33\%$	450v	1.3×10^5	28200	2×10^{-2}	28	0
			2130m	5×10^6	28200	6×10^{-2}	2	0
16	Q25	$50\,\mu m, \sim 50\%$**	404v	1×10^5	8750	1×10^{-2}	3	0
			1811m	8.5×10^6	8750	9×10^{-2}	0	0
17*	Q25	$50\,\mu m, > 50\%$**	413v		14550	1×10^{-2}	11	0
			1860m		14550	9×10^{-2}	0	0

Table A.1: Results summary. Index v means violin-like mode, m - mirror-swinging mode. The noise floor was determined as a ratio of minimal amplitude variation resolvable in the bandwidth 10 Hz near the mode frequency to the mean amplitude obtained for this mode (for the violin-like modes this amplitude corresponds to kT with accuracy better than 30%). $\star$ — test set started right after the makeweight was loaded automatically. $\star\star$ — approximate value, sample got broken.

The results of the noise measurement are presented in the Table A.1. Each record was from 1500 sec to 4000 sec long. We joined the records made for the same sample under the identical conditions in a set. Initially we were able to monitor the amplitude of oscillation on one mode at the time only, so for some samples (Q4 and Q9) the pairs of sets presented, one contains records made on the violin-like mode, another - on the mirror-swinging mode. Later, when the second SR810 lock-in amplifier was installed, amplitudes of both modes were stored simultaneously, thus set number 13 and subsequent contain information about the noise in two modes obtained at the same time.

Some samples were tested under different stresses. These results are represented as a separated sets. For the samples Q9 and Q11 load has been increasing manually, step by step, each time vacuum chamber was open and pumped out again. In the case of samples Q20 and Q22 the electrically driven manipulator described above has been used. Usually, the breaking stress value was measured for each sample when the measurements for it had been completed. The sample Q25 is an exception as it broke off right during the record (hence, the applied stress was about to breaking value). The value of applied stress in the table for this sample is an approximate estimation. It is worth to note that many samples were broken during the preparation, especially when we were trying to apply high (about 50 % of breaking stress) load.

The sensitivity to the variation of the amplitude of the selected modes varies from set to set due to the difference of the cavity finesse, dependence of the background noise on the frequency and optic adjustment imperfection. We characterize it by the noise floor value. It was determined as a ratio of minimal amplitude variation resolvable in the bandwidth 10 Hz (corresponded to 0.1 s measurement time) near the mode frequency to the mean squared amplitude obtained for this mode (for the violin-like modes this amplitude corresponded to kT with metrological accuracy better than 30%).

Each stored record were processed as follows. First, the time intervals when the seismic overcome a predefined limit were excluded. Then the amplitude variations $A_t = A_i - A_{i-1}$ over the unity time interval (time of measurement, in our case $t = 0.1$ s) was obtained and rms amplitude variation has been calculated:

$$\overline{A_t^2} = \frac{\sum (A_t)^2}{N_0} \tag{A.4}$$

here N_0 - total number of unity intervals. For the pure thermal motion the distribution of amplitude variations should be close to normal [11]:

$$P[A_t] \cong \frac{1}{\sqrt{2\pi\sigma}} \exp(-\frac{A_t^2}{2\sigma^2}) \tag{A.5}$$

and $\sigma = \sqrt{\overline{A_t^2}}$. The expected number of intervals where $X \leq A_t < X + \Delta X$ is:

$$N(X, \Delta X) = N_0 \, \Delta X \, P[X + \Delta X/2] \tag{A.6}$$

(it is assumed, that $\Delta X \ll X$).

All points where $A_t^2 > 3\overline{A_t^2}$ were considered as candidate events. Then, if a spike was registered by any monitor channel simultaneously with a candidate event, this event was excluded from the future consideration. We also excluded consequent pairs of candidates which corresponds to single laid-down amplitude value and caused by environment electric

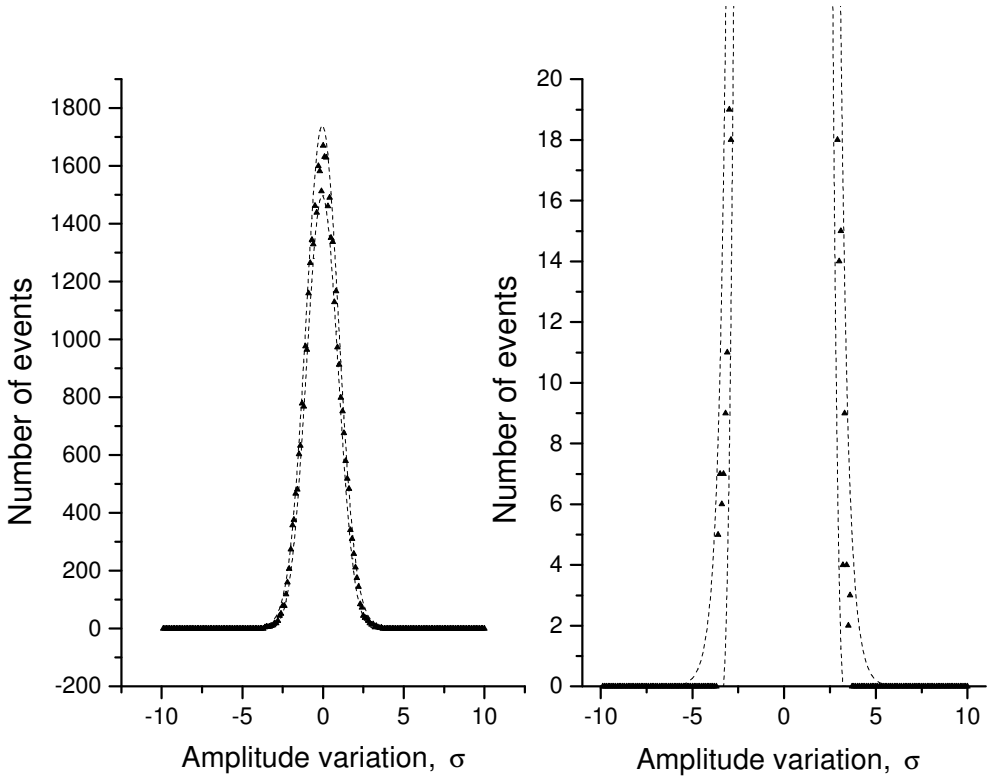

Figure A.5: Left: Histogram for the amplitude variations for one record made for the sample $Q21$. Right: enlarged bottom part.

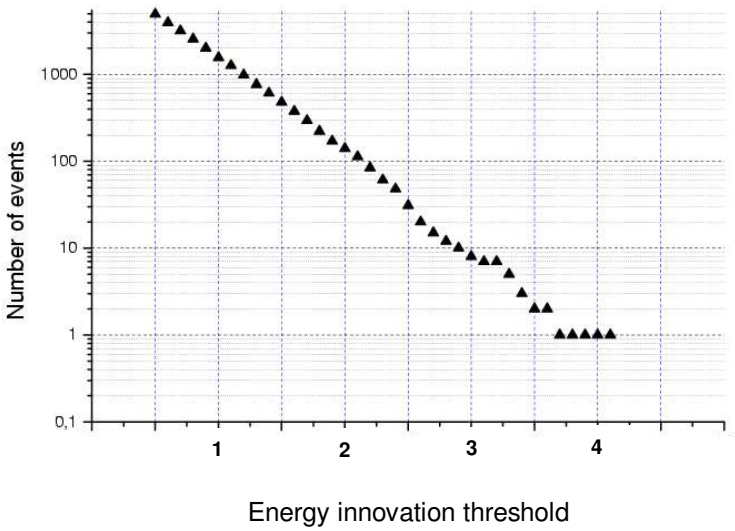

Figure A.6: Cumulative histogram for the energy innovation values (sample Q21). The total number of events when η_i^2 overcomes a threshold is plotted as a function of the threshold value. The deviation from the straight line (that represents exponential distribution) is insignificant, hence there are no evidence of excess noise presence. 5 points at the right end corresponds to only one event when $\eta_i^2 > 4\sigma_\eta$

spikes. Then the data were plotted as a histogram. The typical example is on the figure A.5 ($-10\,\sigma < X < 10\,\sigma$, $\Delta X = \sigma/10$, $N_0 = 45986$). The dash lines bound area there N should be with the probability $P_\alpha > 0.99$ for the given N_0. It is clear, that there are no significant excessive events in the example. The similar results were observed for all records. Total duration of the refined records were about 20 hours for violin-like mode and about 70 hours for mirror-swinging mode.

Quite often the value named *energy innovation* [12] is used for representation of a noise in the oscillatory mode:

$$\eta_i^2 \equiv [A1_i - A1_{i-1}]^2 + [A2_i - A2_{i-1}]^2 \tag{A.7}$$

here $A1_i = A_i sin(\varphi_i), A2_i = A_i cos(\varphi_i)$ are quadrature amplitudes, A_i and φ_i - amplitude and phase, respectively. In fact, η is sensitive to the variation of the oscillator phase as well as its energy. During the first part of our measurements only the values of A_i were stored. Later the possibility to store a pair of quadrature amplitudes instead was implemented. On the figure A.6 the cumulative histogram for the energy innovation obtained for one record made on the sample $Q21$ is presented for comparison purpose.

Conclusion

The results described above demonstrated absence of excess noise in the stressed fused silica fibers at the achieved sensitivity level. From our point of view this can be regarded

as a support of the Advanced LIGO suspension design. Though our samples were only models of this suspension having smaller diameters and extra mirrors inside, one can extrapolate these results to estimate the corresponding amplitude of the Advanced LIGO mirror oscillations:

$$A_L \approx \bar{A}\sqrt{2\,t/\tau^*} \times \frac{m_m}{M_L} \approx 1 \times 10^{-9}\,cm\sqrt{2 \cdot 0.1s/600s} \times \frac{0.02\,g}{4 \times 10^4\,g} \approx 1 \times 10^{-17}cm \quad \text{(A.8)}$$

here M_L is a mass of the Advanced LIGO mirror.

The ultimate displacement sensitivity in this experiment was improved by two orders of magnitude as compared to [9] that allows us to use 10 times smaller measurement time and reach the amplitude variation resolution which corresponds $\simeq 1\%kT$.

To investigate the noise in the suspension with better resolution both the quality factor of violin-like mode and sensitivity of the readout system should be improved.

References

[1] Barish, B. and Weiss, R., Phys. Today, 52 (1999) 44.

[2] B.Abbott, R.Abbott, R.Adhikari, et al. Nucl. Instrum. and Methods in Phys. Research A:517 (2004) 154.

[3] V.B.Braginsky, V.P.Mitrofanov, S.P.Vyatchanin. Rev. Sci. Instrum, 65 (1994) 3771.

[4] A.M.Gretarsson, G.M.Harry, P.R.Saulson, S.D.Penn, W.J.Startin, J.Hough, S.Rowan, G.Cagnoi, Phys.Lett. A 270 (2000) 108.

[5] V.B.Braginsky, V.P.Mitrofanov, K.V.Tokmakov, Phys. Lett. A 218 (1996) 164.

[6] P.Willems, V.Sannibale, J.Weel, V.Mitrofanov, Phys. Letters A 297 (2002) 37.

[7] N.A.Robertson, G.Cagnoli, D.R.M.Crooks, E.Elliffe, J.E.Faller, P.Fritschel, S.Gossler, A.Grant, A.Heptonstall, J.Hough, H.Luck, R.Mittleman, M.Perreur-Lloyd, M.V.Plissi, S.Rowan, D.H.Shoemaker, P.H.Sneddon, K.A.Starin, C.I.Torrie, H.Ward and P.Willems, Class.Quantum. Grav. 19 (2002) 4043.

[8] A.Gillespie and F.Raab, Phys.Lett. A 190 (1994) 213.

[9] A.Yu.Ageev, I.A.Bilenko, V.B.Braginsky. Phys. Lett. A, 246 (1998) 479.

[10] I.A.Bilenko, S.L.Lourie Phys. Lett. A, 305 (2002) 31.

[11] V.B.Braginsky and A.B.Manukin, Measurements of Weak Forces in Physical Experiments, Univ. of Chicago Press, 1977.

[12] A.M.Gretarsson and P.R.Saulson *in press*.

[13] A.M.Gretarsson, G.M.Harry, Rev. Sci. Instrum 70 (1999) 4081.

Appendix B

Nonstationary electrical charge distribution on the fused silica bifilar pendulum and its effect on the mechanical Q

.

Effect of electrical charging of the fused silica test mass on the mechanical Q of various modes has been observed earlier [1, 2, 3, 4]. Degradation in the Q is associated with interaction between charges sitting on the test masses and surrounding bodies, for example, due to Coulomb force. In the previous measurements we have found that the losses associated with charging depended not only on the value of the charge but probably on the state of the charge (for example, the character and distribution of infill of traps, which catch electrical charges). So far there is no good theory which describes the losses associated with charging of the test masses. We continued to study dissipation caused by the charging. In the previous measurements the charge located on the test mass was in the state close to the stationary state. This year we began to study dissipation in the case when the charge was in the nonstationary state.

The Figures presented below illustrate the main results of research which were described in the Summary.

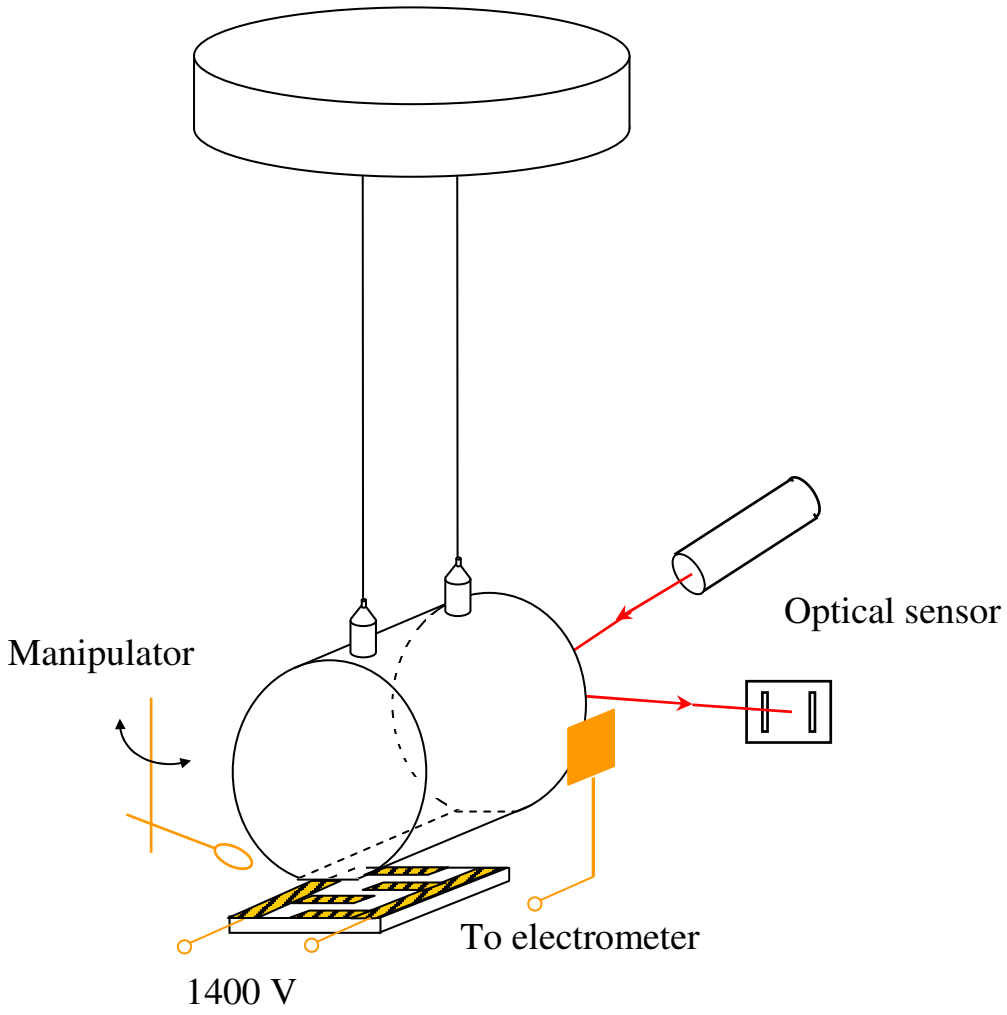

Figure B.1: Schematic of the all fused silica pendulum with additional arrangements used to investigate effects associated with electrical charging of the pendulum bob: the optical sensor for measurement of the bifilar torsion mode amplitude; the plate with electrodes for creation of the electric field; the capacitive probe for monitoring of electrical charge; the manipulator for contact electrification of the cylinder.

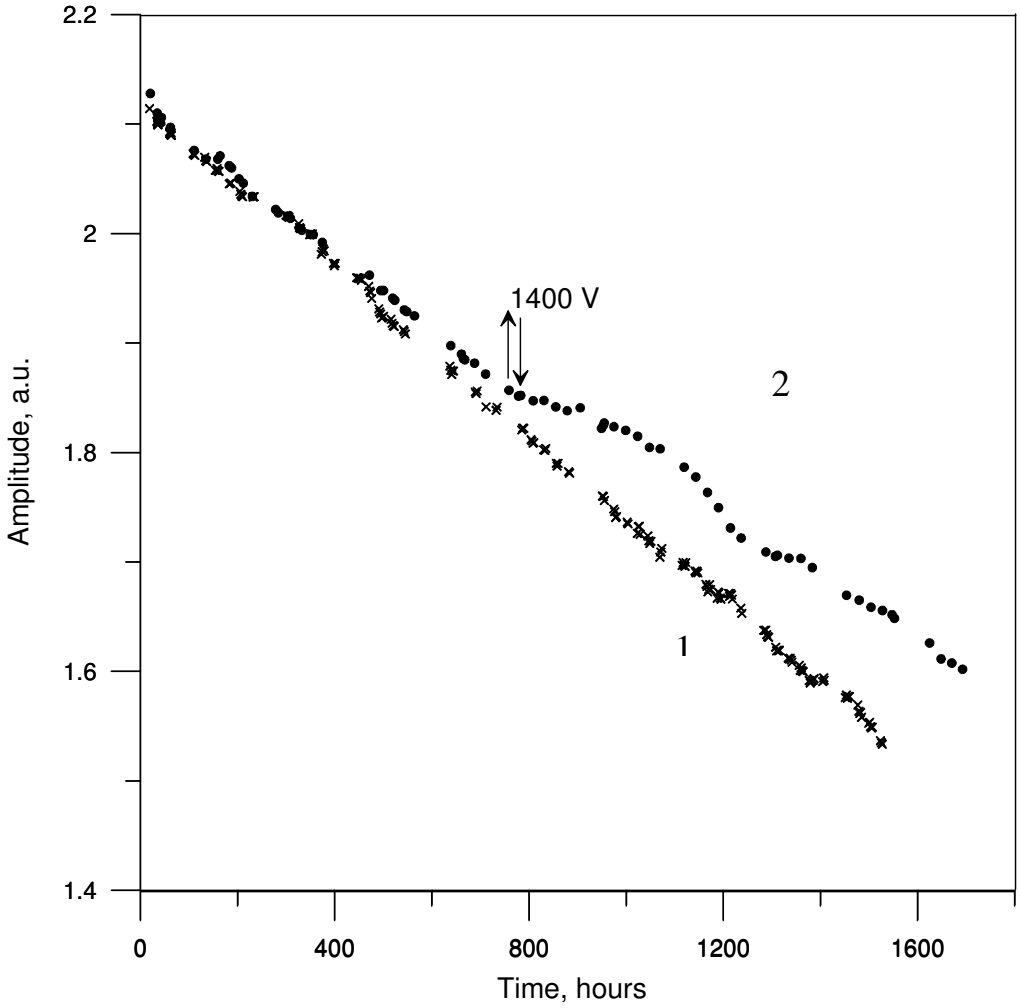

Figure B.2: Free decay of the pendulum amplitude (curve 1). Free decay of the pendulum amplitude in case when the high voltage was applied to the electrodes (curve 2 - application of the voltage during 24 hours is shown by arrows).

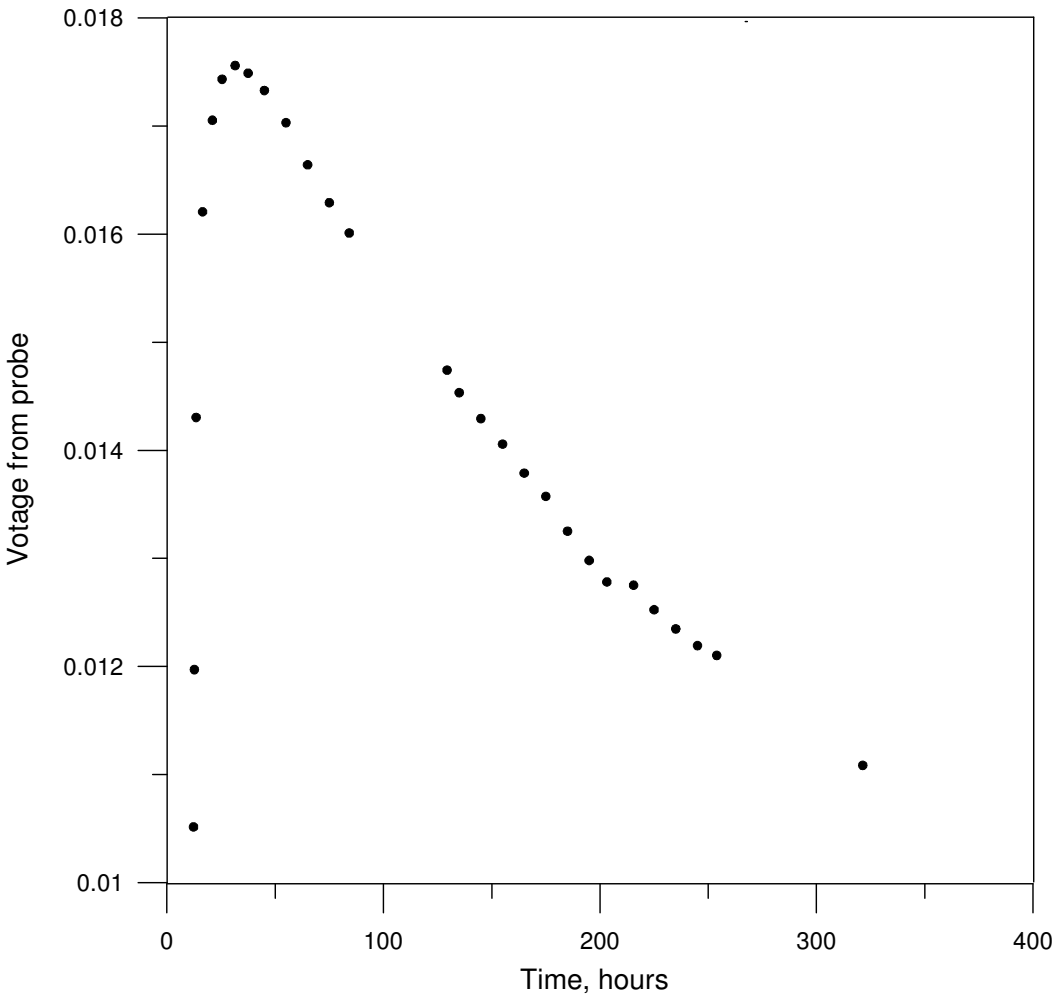

Figure B.3: Time dependence of the probe voltage after electrical charge deposition produced by means of the contact electrification.

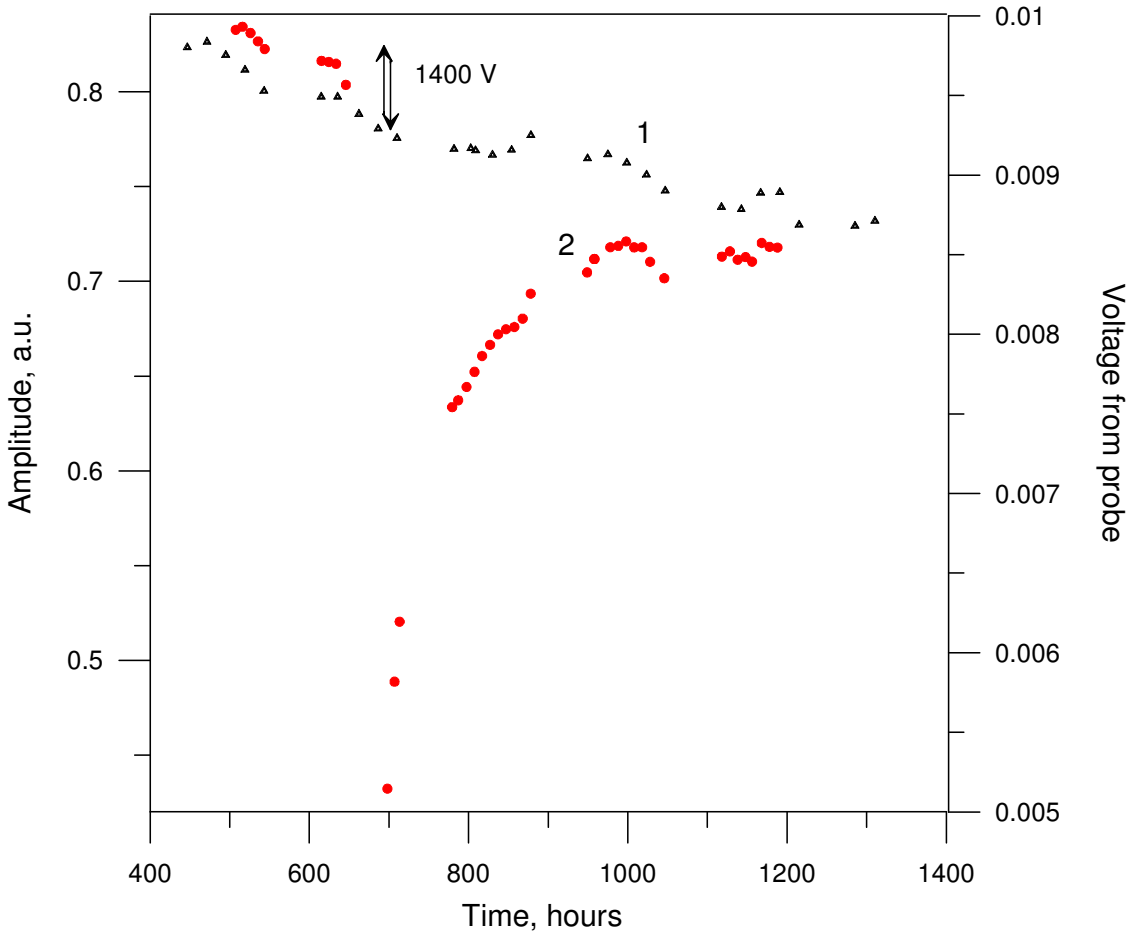

Figure B.4: Fragment of free decay of the pendulum amplitude (run #3) in case when the high voltage was applied to the electrodes (curve 1 - application of the voltage is shown by arrows). Time dependence of the probe voltage (curve 2).

References

[1] S.Rowan, S.M.Twyford, R.Hutchins, and J.Hough, Class. Quantum Grav. **14**, 1537 (1997).

[2] V.P.Mitrofanov, N.A.Styazhkina, K.V.Tokmakov, Physics Letters A **278**, 25 (2000).

[3] M.J.Mortonson, C.C.Vassiliou, D.J.Ottaway, D.H.Shoemaker, and G.M.Harry, Rev. Sci. Instrum. **74** 4840 (2003).

[4] V.Mitrofanov, L.Prokhorov, K.Tokmakov and P.Willems, Class. Quantum Grav. **21**, 1083 (2004).

Appendix C

Corner reflectors and Quantum-Non-Demolition Measurements in gravitational wave antennae

We propose Fabry-Perot cavity with corner reflectors instead of spherical mirrors to reduce the contribution of thermoelastic noise in the coating which is relatively large for spherical mirrors and which prevents the sensitivity better than Standard Quantum Limit (SQL) from being achieved in laser gravitational wave antenna. We demonstrate that thermo-refractive noise in corner reflector (CR) is substantially smaller than SQL. We show that the distortion of main mode of cavity with CR caused by tilt and displacement of one reflector is smaller than for cavity with spherical mirrors. We also consider the distortion caused by small nonperpendicularity of corner facets and by optical inhomogeneity of fused silica which is proposed as a material for corner reflectors.

Introduction

The existing to-day's multi-layer dielectric coating on optical mirrors allows to realize very high resolution experiments (see e.g. [1]). The reflectivity R in the best optical coating has reached the level of $(1-R) \simeq 10^{-6}$ [1, 2, 3] (commercially available $(1-R) \simeq 10^{-5}$), and there are many reasons to expect that further improvement of coating technologies will permit to obtain the value of $(1-R) \simeq 10^{-9}$. With the value of $(1-R) \simeq 10^{-5}$ it is possible to realize the ring down time $\tau^*_{FP} \simeq 1$ sec in 4 km long Fabry-Perot (FP) resonators which are the basic elements in laser interferometer gravitational wave antennae (project LIGO [4, 5]). This relatively large value of τ^*_{FP} permits to have relatively small value of the ratio of $\sqrt{\tau_{av}/\tau^*_{FP}} \simeq 7 \times 10^{-2}$ (if the averaging time $\tau_{av} \simeq 5 \times 10^{-3}$ sec). This ratio is the limit for the squeezing factor which may be obtained if QND procedure of measurement in such FP resonator is used [6, 7]. Such a procedure will allow to circumvent the Standard Quantum Limit (SQL) of sensitivity (see details in [8]).

Few years ago the role of the thermoelastic noise in the bulk of the mirrors was analyzed [9]. This analysis has shown that if the laser beam spot size on the mirror surface is sufficiently large then the small value of the thermal expansion coefficient $\alpha_{SiO_2} \simeq 5 \times 10^{-7}\ K^{-1}$ of fused silica will permit to circumvent the SQL sensitivity by the factor of

$\simeq 0.1$ (if the thermoelastic noise is the only source of noises). The consequent analysis of thermoelastic noise in the coating itself unfortunately predicts that the limit of sensitivity will be close to the SQL of sensitivity [10, 11, 12, 13]. The origin of this obstacle is relatively big numerical value of thermal expansion coefficient $\alpha_{Ta_2O_5} \simeq 5 \times 10^{-6}\ K^{-1}$ of amorphous Ta_2O_5 [13] which is used in the best coatings as well as relatively big number of layers (usually 20-40) which is necessary to have small value of $(1 - R)$. For LIGO project these limitations may be illustrated by the following numerical values. The SQL sensitivity of detectable amplitude of the perturbation of the metric is equal to [14]

$$\sqrt{S_h^{SQL}(\omega)} = \sqrt{\frac{8\hbar}{m\omega^2 L^2}} \simeq 2 \times 10^{-24}\ \mathrm{Hz}^{-1/2}, \tag{C.1}$$

where $m = 40$ kg is mass of test mass, $L = 4$ km is distance between them, $\omega = 2\pi \times 100\ \mathrm{s}^{-1}$ is observation frequency. Here and below the estimates are calculated for numerical parameters listed in Appendix C. At the same time, according to the measurement [13], the limit of sensitivity of such an antenna only due to the thermoelastic noise in the multi-layer $Ta_2O_5 + SiO_2$ coating on SiO_2 substrate has to be between [10]

$$\sqrt{S_h^{TD\,coat}(\omega)} \simeq \left(0.6 \div 1.4\right) \times 10^{-24}\ \mathrm{Hz}^{-1/2} \tag{C.2}$$

The goal of this article is to present the analysis of another version of optical FP cavity where the "contribution" of the thermoelastic noise in coating is substantially reduced. The key idea of this version is based on concept of corner optical reflector (tri-hedral or two-hedral prism). These types of reflectors were well known among the jewelers at least from 16-th century (see e.g. autobiography by Benvenutto Cellini [15]). In the 70-s of the previous century corner reflectors (CR) installed on the Moon allowed to test the principle of equivalence for the gravitational defect of mass by laser ranging [16]. Here we propose to substitute mirrors with finite value of surface curvature (see fig.C.1 a) by 3 facets (fig.C.1 b) or 2 facets (see fig.C.1 c) corner reflectors (CR) manufactured from fused silica. For the same radius R_b of laser beam the mass of CR is about the same value as cylindrical mirrors (with height about equal to radius of cylinder) especially if idle parts of CR is removed. For example for 2 facets CR the size of foot surface has to be about 45×45 cm^2 with total test mass about 40 kg (the same as planned in advanced LIGO).

In the proposed scheme the stability of optical mode is provided by surfaces lens shaping of each CR foot (as shown in fig.C.2a). For reflectors manufactured from fused silica the total internal reflection inside the reflectors is possible because refraction index $n_{SiO_2} = 1.45$ is large enough (due to Snellius law): $n_{SiO_2}\sqrt{2/3} > 1$ for 3 facets reflector or $n_{SiO_2}\sqrt{1/2} > 1$ for 2 facets reflector.

In section C we consider the modes of ideal cavity (fig.C.2) and the distortion of the main mode structure caused by small perturbations of different kinds: tilt angle θ (fig. C.3), displacement δx of one reflector (fig. C.4), expose angle ϵ (fig.C.5).

In section C we compare these perturbations for cavities with spherical mirrors and with corner reflectors and give numerical estimates for the particular case of laser beam radius $R_b \simeq 6$ cm (intensity of beam decreases as e^{-1} at distance R_b from center) which is planned for Advanced LIGO. Distortions of mode are undesirable in high accuracy spectroscopic measurements because they may produce additional noise. For example, in

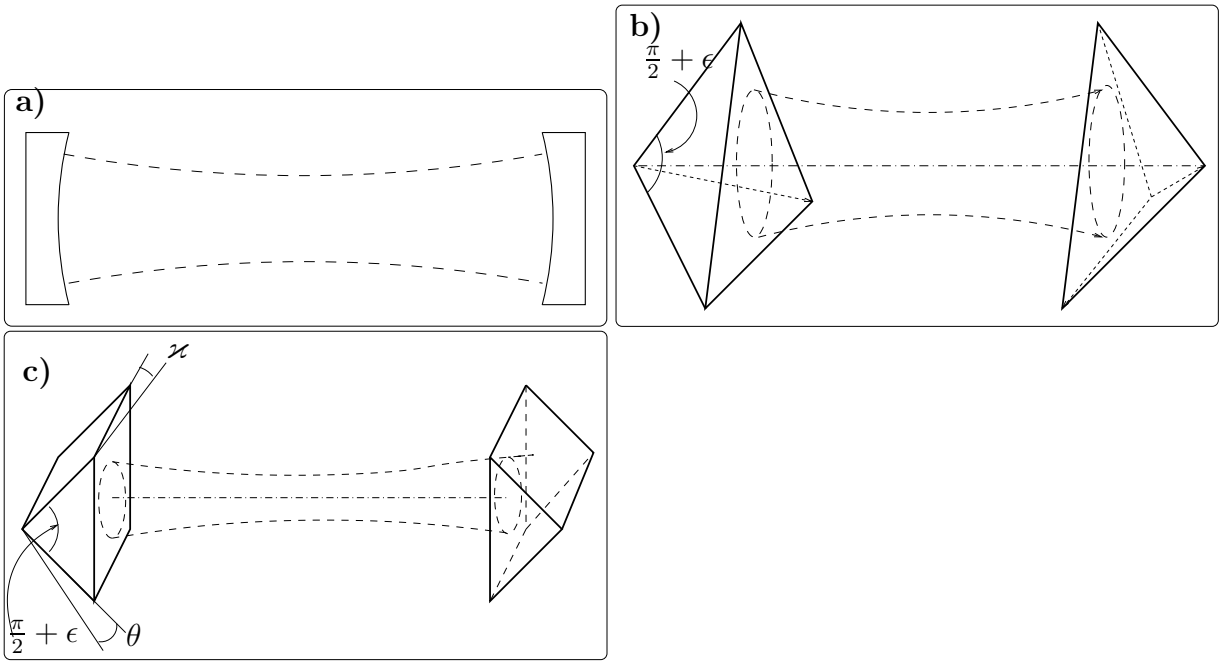

Figure C.1: We propose to replace mirrors with finite value of surface curvature (a) by 3 facets "triprism" type CR (b) or 2 facets "roof" type CR (c).

laser gravitational wave antenna the light beams from two independently perturbed FP cavities (placed in each arm of Michelson interferometer) will not produce completely zero field at the dark port after the beam splitter. It is equivalent to additional noise at the dark port.

In section C we consider the different sources of optical losses of CR and show that they can be at level $(1-R) \simeq 10^{-5}$.

In cavity with CRs it is necessary to use nevertheless relatively thin anti-reflective coatings (2 – 4 layers) on lense shape foot. It has to be done to keep the value $(1-R)$ at the level $\simeq 10^{-5}$. Because this coating is substabtialy thiner than typical high reflective one (20 – 40 layers) used in curved mirrors, thermoelastic noise may be depressed by the factor ~ 10 i.e. about one order less than SQL (the estimate (C.2) is given for 38 layers). The "fee" for use of CR is the additional thermo-refractive noise [17] (fluctuations of temperature produce the fluctuations of refractive index) because light beam is traveling inside the corner reflector. However we will show in section C that it is several times smaller than SQL for reflectors manufactured from fused silica. Important that this thermo-refractive noise rapidly decreases with increasing of radius R_b of beam spot as $\sim R_b^{-2}$.

In cavity with CR the thermoelastic noise in the facets remains, but as mentioned above if the reflectors are manufactured from fused silica and the beam spot is large enough (see e.g. [10]) then it is possible to circumvent SQL.

The Distortions of main mode in FP cavity with CR

Firstly, we consider FP cavity with two identical perfect corner cube reflectors with three reflecting facets (see fig.C.1b): i) the corner angles between the facets are exactly equal

to $\pi/2$; ii) the top points of the reflectors are located exactly on common optical axis; iii) the "foots" of the reflectors have slight curvatures (shape of a lens surface as shown in fig. C.2a) and they are perpendicular to the axis. Then we consider the distortion of mode in this cavity caused by different perturbations.

FP resonator with perfect CR

We can consider that each CR consists of reflector with plane foot surface together with spherical lens as shown in fig.C.2b. The CR produces mirror transformation, i.e. light beam which enters the reflector in point C is transformed into the beam leaving the reflector in point C'. Using Fresnel integral one can obtain the integral equations for calculations of eigenmode distribution:

$$e^{ikL} \int G_0(\vec{r}_1, \vec{r}_2)\, \Phi_2(\vec{r}_2)\, d\vec{r}_2 = \lambda \tilde{\Phi}_1(\vec{r}_1), \tag{C.3}$$

$$e^{ikL} \int G_0(\vec{r}_1, \vec{r}_2)\, \Phi_1(\vec{r}_2)\, d\vec{r}_1 = \lambda \tilde{\Phi}_2(\vec{r}_2), \tag{C.4}$$

$$d\vec{r}_1 = dx_1\, dy_1, \quad d\vec{r}_2 = dx_2\, dy_2.$$

Here functions $\Phi_1(\vec{r}_1)$ and $\Phi_2(\vec{r}_2)$ describe distribution of complex field amplitude emitted from imagine flat foot surfaces of reflector 1 (left) and reflector 2 (right) correspondingly just under lenses in planes AA' and BB'. L is the optical path between reflectors (including path inside the reflector). Evidently phase fronts coincide with planes AA' and BB' so that phases of functions Φ_1 and Φ_2 are constants. The notation $\tilde{\Phi}_1(\vec{r}_1)$ means the "mirror" transformation (produced by 3 facets CR) relative to the optical axis[1]:

$$\tilde{\Phi}_1(\vec{r}_1) = \Phi_1(-\vec{r}_1), \qquad \tilde{\Phi}_2(\vec{r}_1) = \tilde{\Phi}_2(-\vec{r}_1)$$

The kernel G^0 is:

$$G_0(\vec{r}_1, \vec{r}_2) = -\frac{i}{2\pi} e^{i\left(\frac{(\vec{r}_1 - \vec{r}_2)^2}{2} - h_1(\vec{r}_1) - h_2(\vec{r}_2)\right)}, \tag{C.5}$$

$$h_1 = \frac{r_1^2}{r_h^2}, \qquad h_2 = \frac{r_2^2}{r_h^2} \tag{C.6}$$

Here we use the dimensionless transversal coordinates $\vec{r}_1$ and $\vec{r}_2$ (at planes AA' and BB') which can be expressed in terms of physical coordinates $\vec{R}_1$ and $\vec{R}_2$ as

$$\vec{r}_1 = \frac{\vec{R}_1}{b}, \qquad \vec{r}_2 = \frac{\vec{R}_2}{b}, \qquad b = \sqrt{\frac{L}{k}},$$

where k is wave vector, h_1 and h_2 are additional phase shifts produced by spherical lenses at each reflector foot. It is easy to see that for spherical lenses the set of eigenmodes Φ_1^{mn}, Φ_2^{mn} and their eigenvalues λ_{mn} (below we assume $\lambda_{00} = 1$) of our FP cavity are

[1]For 2 facets reflector we have mirror transformation only relatively x coordinate: $\tilde{\Phi}_1(x, y)) = \Phi_1(-x, y)$

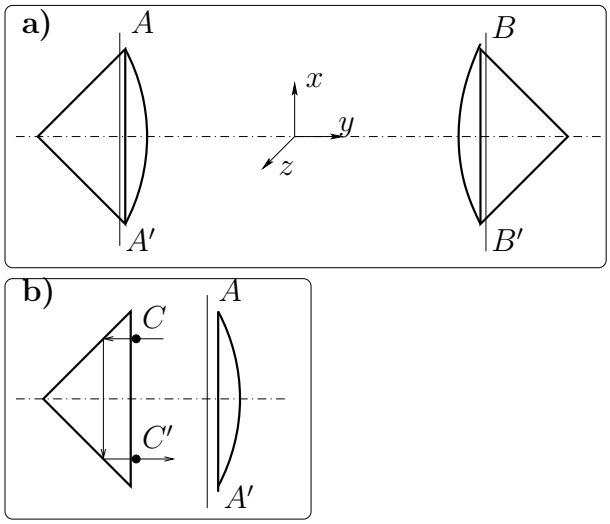

Figure C.2: a). The perfect alignment of CR assembling cavity. b). Each reflector can be regarded as reflector with plane "foot" plus a lens.

described by generalized Gauss-Hermite functions:

$$\Phi_1^{mn} = \phi_m(x)\phi_n(y), \tag{C.7}$$

$$\Phi_2^{mn} = (-1)^{-m+n}\Phi_1^{mn} = \tilde{\Phi}_1^{mn} \tag{C.8}$$

$$\phi_m(x) = \frac{1}{\sqrt{r_L}\,\sqrt{\sqrt{\pi}\,2^m\,m!}}\,H_m\left(\frac{x}{r_L}\right)\times \tag{C.9}$$

$$\times \exp\left[-i(m+1/2)\psi - \frac{x^2}{2r_L^2}\right],$$

$$\lambda_{mn} = e^{2i(m+n)\psi}, \qquad \psi = \arctan\left(\frac{1}{2r_0^2}\right),$$

$$h_1(r) = h_2(r) = \frac{r^2}{2r_h^2}, \quad 2r_L^2 = 2r_0^2 + \frac{1}{2r_0^2} \tag{C.10}$$

$$2r_h^2 = (2r_0^2)^2 + 1 = 2r_L^2\,2r_0^2. \tag{C.11}$$

Here $H_m(t)$ is the Hermite polynomial of the order m, r_0 and r_L are the radii of beam in the waist and at the lens correspondingly. It is useful to write down the expressions for $r_0,\ r_L,\ r_h$ using g-parameter [18] (R^* — is the radius of wave front curvature (in cm) just after the propagation of beam through the lens outside of the reflector):

$$g = 1 - \frac{L}{R^*}, \quad r_0^2 = \frac{1}{2}\sqrt{\frac{1+g}{1-g}}, \tag{C.12}$$

$$r_L^2 = \frac{R_b^2}{b^2} = \frac{1}{\sqrt{1-g^2}}, \quad r_h^2 = \frac{R^*}{L} = \frac{1}{1-g}, \tag{C.13}$$

$$\sin 2\psi = g, \quad \cos 2\psi = \sqrt{1-g^2}. \tag{C.14}$$

We are interested in the main mode $\Phi_1^{00}(x,y)$ of resonator (amplitude distributions of left and right reflectors obviously coincide with each other for the main mode: $\Phi_1^{00}(x,y) = \Phi_2^{00}(x,y)$).

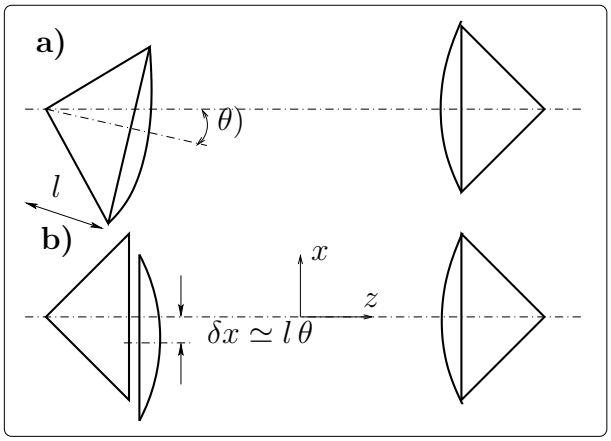

Figure C.3: a). Small tilt of the left CR around its head. b) This tilt is equivalent to untilted reflector and displaced lens.

Distortion due to the Tilt of CR

Here we consider the main mode $\breve{\Phi}_1^{00}(x,y)$ perturbed due to tilt misalignment shown in fig. C.3a. We expand the perturbed main mode into series over the set of unperturbed modes limiting ourselves to the lowest (dipole) approximation:

$$\breve{\Phi}_1^{00}(x_1,y_1) \simeq \Phi_1^{00}(x_1,y_1) - \alpha_1^{\text{tilt}}\Phi_1^{10}(x_1,y_1), \tag{C.15}$$

$$\breve{\Phi}_2^{00}(x_2,y_2) \simeq \Phi_2^{00}(x_2,y_2) + \beta_1^{\text{tilt}}\Phi_2^{10}(x_2,y_2). \tag{C.16}$$

The tilt of CR around its head through a small angle of θ can be considered as untilted reflector with lens displaced a small distance $\delta x \simeq l\theta$ perpendicular to optical axis (l is the dimensionless distance between the foot and head of CR, it is illustrated in fig. C.3b). For this case the perturbations of the main mode can be described by dipole coefficients defined in (C.15, C.16):

$$\alpha_1^{\text{tilt}} \simeq l\theta\,\frac{g\,(1-g)}{\sqrt{2}\,(1-g^2)^{3/.4}}, \tag{C.17}$$

$$\beta_1^{\text{tilt}} \simeq l\theta\,\frac{(1-g)\left[\cot\left(\psi\right)-i\right]}{2\sqrt{2}\,(1-g^2)^{1/4}}, \tag{C.18}$$

$$|\beta_1^{\text{tilt}}| \simeq \frac{l\theta}{2}\sqrt[4]{\frac{1-g}{1+g}} \tag{C.19}$$

See details of calculations in Appendix C.

Note that distortion produced by tilt of two facets CR around perpendicular axes (angle $\varkappa$ on fig. C.1c) can be described by the same formulas as tilt of spherical mirror.

The Distortion due to the Displacement of CR

One CR can be displaced by a small distance δx so that optical axes of reflectors do not coincide with each other as it is shown in fig. C.4. For this case the perturbations of the main mode can be described by dipole coefficients defined by formulae (C.15, C.16).

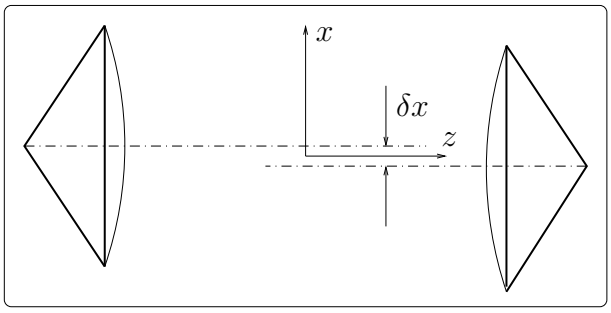

Figure C.4: One CR is displaced relative to another one.

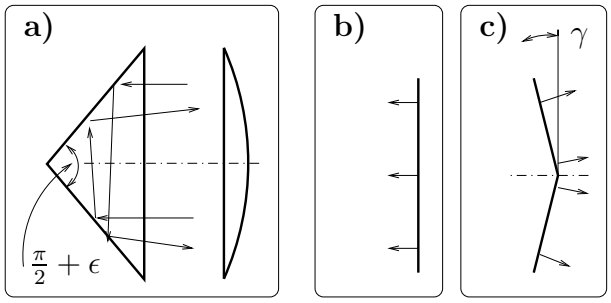

Figure C.5: (a). Expose perturbation: the angle between facets of corner reflector differs from direct angle by a small value of ϵ. It produces the transformation of incident plane wave front (b) into a "broken" front of reflected wave (c).

Denoting the dipole coefficients as α_1^{displ} and β_1^{displ} one can obtain:

$$\alpha_1^{\text{displ}} = \beta_1^{\text{displ}} \simeq \frac{-\delta x}{2\sqrt{2}} \left(\frac{-2ig}{\sqrt[4]{1-g^2}} + \sqrt[4]{1-g^2} \right) \tag{C.20}$$

See details of calculations in Appendix C.

The Distortion of Expose Angle

Here we consider the case when, for example the left reflector (2-hedral prism shown in fig. C.1c) has a non-perfect perpendicular facets, so that expose angle between them differs from $\pi/2$ by a small angle of ϵ (fig. C.5a). Then the plane front of incident wave after reflection from the reflector is transformed into a broken surface consisting of two plane parts declined to the incident wave front by an angle of $\gamma = 2\epsilon$ as shown in fig. C.5b,c.

This statement is also correct for tri-hedral reflectors (shown in fig. C.1b) with the exception of numerical factor: if only one facet is declined by angle of ϵ from the normal position (and other two facets are non-perturbed) the angle γ will be equal to $\gamma = 2\epsilon\sqrt{2/3}$.

Again we can expand the perturbed main mode over the set of unperturbed modes of ideal cavity keeping only the lowest first-order non-vanishing term of expansion:

$$\breve{\Phi}_1^{00}(x_1, y_1) \simeq \Phi_1^{00}(x_1, y_1) + \alpha_2^{\text{expose}} \Phi_1^{20}(x_1, y_1), \tag{C.21}$$

$$\breve{\Phi}_2^{00}(x_2, y_2) \simeq \Phi_2^{00}(x_2, y_2) + \beta_2^{\text{expose}} \Phi_2^{20}(x_2, y_2) \tag{C.22}$$

(due to the symmetry of this kind perturbation the dipole term is null). Calculation gives the following value for α_2:

$$\alpha_2^{\text{expose}} \simeq \frac{i\gamma L}{4\sqrt{2}\,\pi\, b \sqrt[4]{1-g^2}} \times \frac{\left(g + i\sqrt{1-g^2}\right)^2}{i\, g\, \sqrt{1-g^2}} \tag{C.23}$$

$$|\alpha_2^{\text{expose}}| = |\beta_2^{\text{expose}}| \simeq \frac{L\gamma}{4\sqrt{2}\,\pi\, b\, g(1-g^2)^{3/4}} \tag{C.24}$$

See details in Appendix C.

Comparison of FP cavities with CR and with spherical mirrors

Recall that uncontrollable perturbations of the mode produce additional noise: in laser interferometer gravitational antenna the signal at dark port will contain additional noise with power proportional to the square of distortion coefficients $\sim |\alpha|^2, |\beta|^2$. In this section we compare numerically the distortion of the main mode in traditional FP cavity with spherical mirrors (SM cavity) with FP cavity assembled by CR (CR cavity).

The distortion of the main mode in SM cavity caused by small displacement and tilt of one mirror can be also described by coefficients α_1 of expansion (C.15)[20, 21]:

$$\alpha_1^{\text{tilt, Sph}} = \frac{1}{\sqrt{2}\,(1-g^2)^{3/4}} \left(\frac{\theta\, L}{b}\right), \tag{C.25}$$

$$\alpha_1^{\text{displ, Sph}} = \left(\frac{(1-g)^{1/4}}{\sqrt{2}(1+g)^{3/4}}\right) \delta x \tag{C.26}$$

For estimates for both SM and CR cavity we use the parameters of cavity proposed for Advanced LIGO [20]:

$$r_L = 6/2.6 \simeq 2.3, \quad g = 0.982. \tag{C.27}$$

These parameters correspond to the radius of laser beam R_b at the reflector surface of about $R_b \simeq 6$ cm. Assuming additionally that dimension length l^* from foot to top is equal to $l^* = 20$ cm, i.e.

$$l = \frac{20\,\text{cm}}{b} \simeq 7.7\,,$$

and dimension displacement $\delta x^* = b\,\delta x$ we obtain the following estimates for SM cavity:

$$\alpha_1^{\text{tilt, SM}} = 0.013 \left(\frac{\theta}{10^{-8}}\right), \tag{C.28}$$

$$\alpha_1^{\text{disp, SM}} = 0.0059 \left(\frac{\delta x^*}{0.1\text{ cm}}\right) \tag{C.29}$$

and for CR cavity:

$$\alpha_1^{\text{tilt, CR}} = 1.2 \times 10^{-7} \left(\frac{\theta}{10^{-8}}\right), \tag{C.30}$$

$$\alpha_1^{\text{displ, CR}} = 0.06 \left(\frac{\delta x^*}{0.1\text{ cm}}\right), \tag{C.31}$$

$$\alpha_2^{\text{expose}} = 0.11 \left(\frac{\gamma}{10^{-6}}\right). \tag{C.32}$$

We see that CR cavity is substantially more stable to tilt and less stable to displacement than SM cavity. However, the total requirements for SM cavity looks more tough if one compares the estimates (C.28 and C.31). Indeed to keep control of tilt in SM cavity with accuracy $\theta \simeq 10^{-8}$ rad (see (C.28)) one has to operate the positioning system with accuracy about $lb\,\theta \simeq 2 \times 10^{-6}$ cm. But the same level of displacement distortion in CR cavity (see (C.31)) one can obtain by displacement control with much lower accuracy: ≤ 1 mm only (!).

The requirement for an expose angle in CR cavity looks also acceptable: for accuracy of manufacturing $\epsilon \simeq 3{\times}10^{-7}$ (commercially available prisms have $\epsilon \simeq \pm 1{\times}10^{-5}$) and hence $\gamma = 2\epsilon\sqrt{2/3} \simeq 4.9{\times}10^{-7}$ we have to take into account that three angles between facets (increasing factor $\sqrt{3}$) in each of two tri-hedral reflector (one more increasing factor $\sqrt{2}$) may be independently perturbed (so the total increasing factor is equal to $\sqrt{3}{\times}\sqrt{2} = \sqrt{6}$):

$$\sqrt{\sum \left(\alpha_{2,\,i}^{\text{expose}}\right)^2} \simeq \sqrt{6}\,\alpha_2^{\text{expose}} \simeq 0.13$$

Optical inhomogeneity is one more source of perturbation which is specific to CR: the refraction index of fused silica (which CR is manufactured from) changes over the value of $\delta n \simeq 2 \times 10^{-7}$ along the length $\Delta l \simeq 10$ cm [22]. To estimate negative influence of this effect we can consider the model task using the fact that distance scale Δl of refraction index perturbation is about the dimension bl of the reflector. Let one half of corner reflector has a perturbed refraction index $n+\Delta n(x)$ which depends on a transversal coordinate x only:

$$\Delta n(x) = \begin{cases} \Delta n & = -\delta n \left(1 - \frac{x}{l}\right) \quad \text{if} \quad x > 0, \\ \Delta n & = 0 \qquad\qquad\quad \text{if} \quad x \leq 0 \end{cases} \tag{C.33}$$

In this case the beam after reflection from such a reflector will have a broken wave front as shown in fig. C.5c with angle

$$\gamma = \frac{\delta n}{4n} \tag{C.34}$$

Hence one can estimate the value of perturbation due to inhomogeneity using formula (C.24). It is obvious that for perturbation with another dependence of Δn on space coordinates the formula (C.34) must change this estimate by the factor of about unity or slightly larger. So for estimates we use the 4 times greater value of γ than (C.34). In that case for two reflector with independently perturbed refraction index (factor $\sqrt{2}$) we obtain:

$$\gamma = \frac{\sqrt{2}\,\delta n}{n} \simeq 2 \times 10^{-7}, \quad \alpha_2^{\text{inhomo}} \simeq 0.011 \tag{C.35}$$

The two last kinds of perturbations (expose angle and inhomogeneity) depend only on manufacturing procedure and there is a hope they can be decreased due to the improvement of manufacturing culture.

The optical losses

The loss coefficient for CR cavity must be small — about 10 ppm. We consider the following sources of losses.

Fundamental losses on edge are produced by diffraction on edge where two facets meet. Qualitatively it can be described as two surface waves outside CR (bounded with waves inside due to complete internal reflection) meet at edge producing diffractional scattering (we acknowledge to F.Ya.Fhalili pointed out the existtence of this kind losses).

To our best knowledge nobody performed rigorous analysis of this problem. So we propose the consideration to estimate this effect: (a) using the formulas for complex coefficient of reflection for plane wave from plane infinite boundary between two media for the case of internal reflection (see e.g. [23]) one can construct the solution *inside* CR; (b) using the boundary condition one can obtain the fields along *outside* surface of CR; (c) applying Green's formula one can calculate the radiation field in far wave zone and total diffractional power. The most vulnerable for critics item of this consideration is (a) — applying the formulas for infinite boundary to corner configuration.

We apply this consideration for the case of incident wave polarized along edge of CR of "roof" type (fig. C.1c). For this particular case (with obvious assumption that magnetic permittivity $\mu = 1$) the all field components of constructed solution are smooth inside CR and on outside surface CR. Our calculation gives the following loss coefficient:

$$(1 - R)_d \simeq \frac{0.4\lambda}{R_b} \simeq 0.7 \times 10^{-5} \tag{C.36}$$

where λ is the optical wavelength, (see details in Appendix C).

Note that our consideration of incident wave polarized perpendicular to the edge of CR allows to construct smooth solution inside CR but this solution on the outside surface will have break of components of electrical fields at the edge. Thus to get a reliable confirmation of the approximatetive estimate (C.36) it is necessary either to find a rigorous analytical solution of this problem or to perform straightforward numerical calculation.

The losses on non-perfect edge is produced by scattering of the plane optical wave on the non-perfect "ridges" where two facets meet. The edge of facets intersection with uncontrollable width of $\Delta s \leq 0.5$ μm will produce optical losses which can be roughly estimated as following:

$$(1 - R)_{\rm non-perfect} \leq \frac{\Delta s}{R_b} \simeq 0.8 \times 10^{-5}$$

In other words it satisfies our initial condition to obtain $\tau^*_{\rm FP} \simeq 1$s.

Optical losses of material. Internal optical losses in purified fused silica at the level $\gamma_{\rm loss} \simeq 0.5$ ppm/cm [19] give the loss coefficient about

$$(1 - R)_{opt.loss} \simeq \gamma_{\rm loss} 2bl \simeq 0.8 \times 10^{-5}$$

Losses in anti reflective coating. As we mentioned in Introduction it will be necessary to use anti reflective coating on the bottom surfaces of CR. Calculations which we omit here shows that to keep the value of $(1 - R)$ at the level $\sim 10^{-5}$ it is sufficient to use 2-4 anti reflective layers of coating.

Thermo-refractive noise

The origin of thermo-refractive noise is thermodynamic (TD) fluctuations of temperature which produce fluctuations of phase of light traveling inside the CR through dependence of refractive index n on temperature T: $\beta = dn/dT \neq 0$ [17]. One can estimate TD temperature fluctuations using the model of infinite layer with width l_c ($0 \leq z \leq l_c$). We additionally assume that layer is in vacuum and its both surfaces are thermally isolated (thermal radiation in accordance with Stefan-Boltzmann law is so small that this assumption is quite correct). If light (Gaussian beam) with radius R_b travels through the layer perpendicular to its surface the fluctuations φ of light phase during time τ will be defined by TD temperature fluctuations u averaged over the cylinder $\pi R_b^2 l_c$:

$$\varphi = k l_c \, \beta \, \sqrt{\langle \bar{u}^2 \rangle_\tau}, \quad k = \frac{2\pi}{\lambda}. \tag{C.37}$$

Subscript τ means that we are interested in *variation* of temperature during observation time τ.

The total variation of TD temperature fluctuations is equal to

$$\langle \bar{u}^2 \rangle = \frac{k_B T^2}{\rho C \, \pi R_b^2 l_c}$$

where k_B is the Boltzmann constant, ρ is density, and C is the specific heat capacity. Then the variation of temperature over the small time τ (adiabatic approximation) must be about $\langle \bar{u}^2 \rangle_\tau \simeq \langle \bar{u}^2 \rangle \times \tau/\tau^*$ where $\tau^* = \rho C R_b^2/\kappa$ is thermal relaxation time of our cylinder through lateral surface (base surfaces of cylinder are thermo isolated), κ is thermal conductivity. Here we assume that $\tau \ll \tau^*$. This result can be rewritten in form

$$\langle \bar{u}^2 \rangle_\tau = \frac{k_B T^2}{\rho C \, \pi R_b^2 l_c} \times \left(\frac{r_T^2}{R_b^2} \right), \quad r_T = \sqrt{\frac{\kappa \tau}{\rho C}} \ll R_b, \; l$$

where r_T is thermal diffusive length for the time τ.

Equating $\langle \bar{u}^2 \rangle_\tau \simeq S_{\bar{u}}(\omega) \, \Delta\omega$ we can obtain the estimate for spectral density $S_{\bar{u}}(\omega)$ of averaged temperature putting $\omega \simeq \Delta\omega \simeq 1/\tau$.

The accurate expressions for these spectral densities $S_u(\omega)$ and $S_\varphi(\omega)$ of temperature fluctuations and phase fluctuations correspondingly are the following

$$S_{\bar{u}}(\omega) \simeq \frac{4 k_B T^2 \kappa}{(\rho C)^2 l_c} \, \frac{1}{\pi R_b^4 \omega^2}, \tag{C.38}$$

$$S_\varphi(\omega) \simeq \frac{4 \beta^2 k^2 l_c k_B T^2 \kappa}{(\rho C)^2} \, \frac{1}{\pi R_b^4 \omega^2} \tag{C.39}$$

for adiabatic case, i.e. for $\omega \gg \frac{\kappa R_b^2}{\rho C}$.

One can easy check that our estimate differs from accurate expression (C.38) for $S_{\bar{u}}(\omega)$ only by the factor of about unity. In Appendix C we present derivation of general expression for adiabatic and non-adiabatic cases.

The formulae (C.38, C.39) allows to recalculate thermo-refractive fluctuations into the fluctuations of dimensionless metric h (which usually describes the sensitivity of laser gravitational antennae): $h = \varphi/(kL)$, where L is cavity length. It is useful to estimate

its spectral density $S_h(\omega)$ for parameters of laser gravitational antenna (advanced LIGO) presented in Appendix C and $l_c = 10$ cm:

$$\sqrt{S_h(\omega)} \simeq 0.5 \times 10^{-24} \text{ Hz}^{-1/2}. \tag{C.40}$$

It is about 4 times smaller than the sensitivity of Standard Quantum Limit (C.1) which is planned to achieve in Advanced LIGO [19]. Important that this thermo-refractive noise rapidly decreases with increase of beam radius: $\sqrt{S_h(\omega)} \sim R_b^{-2}$. Thus the using so called "mesa-shaped" beams [20, 21] (having flat distribution in the center and fall to zero more quickly than Gaussian distribution at the edges) with larger radius will allow to decrease thermo-refractive noise by several times. For example using the 45×45 cm^2 foot of CR and $R_b = 10$ cm with mesa shape distribution of the intensity of light in the beam one may expect the gain of sensitivity for $\sqrt{S_h(\omega)}$ approximately one order better than $\sqrt{S_h^{SQL}(\omega)}$.

Conclusion

The presented analysis of FP cavity with two CR (instead of mirrors) has to be regarded as an example of cavity in which thermoelastic noise in the coating may be substantially decreased and which permits to circumvent substantially the SQL of sensitivity and also to have $(1 - R) \approx 10^{-5}$.

We have shown that CR cavity is considerably more stable than cavity with spherical mirrors relative to tilt and displacement distortion. The distortion due to expose angle of CR is not so small but it depends only on manufacturing procedure, and there is a hope to decrease it due to improvement of manufacturing culture.

There does exist another argument in favor of using CR in FP resonators. The very recent measurements performed by LIGO collaborators from University of Glasgow, Stanford University, Iowa State University, Syracuse University and LIGO Lab have shown that multi-layer coating also decreases the quality factors of mirrors internal modes [24]. This effect may substantially increase the Brownian component of the noise in the mirror itself and thus decrease the sensitivity of LIGO antennae (see details on Brownian moise in coating in [25, 26, 27, 28, 29, 30]).

At the same time it is likely that there does exist other version of cavity free from thermoelastic noise in coating, probably more easy to implement which evidently deserves similar in-depth analysis. One of the "candidates" is a cavity with unusual reflective coating: each layer of it has to have the same small value of thermal expansion as fused silica. Unfortunately the technology which may provide it is not yet invented.

In the above analysis we have limited ourselves to the calculations of the cavity properties itselves and did not discuss the coupling of cavity with pumping laser and readout system. This analysis has to be done especially because the readout system may be an intra-cavity one [8] and because special attention has to be paid to the possible specific deformation of the main mode distribution in FP cavity with CR. One of several possible ways to realize the coupling of the mode with pumping source may be based on the existence of the evanescent optical field "outside" the surface of the facets. In this case it will be evidently necessary to use very thin dielectric grating on the surface of the facet.

We have not also discuss the polarization characteristics of CR. For example it is known that the phase shift of wave reflected from plane surface depends on polarization [23]) and hence the FP cavity with 2-facets CR will have slightly different eigen frequencies for waves

with polarization along and perpendicular to edge of CR. The additional problem to be analyzed is the polarization characteristics of 3-facets CR.

It seems that the CR cavity for Advanced LIGO have to be used not for modes with Gaussian distribution of power over the cross section but for so called "mesa-shaped" [20, 21] mode with flat distribution in the center and fall to zero more quickly than Gaussian distribution at the edges. For "mesa-shaped" modes the profile of "lenses" (h_1 and h_2 in C.5) on the foot of the corner reflector must have special dependence on radius calculated in [20, 21].

It is worth noting that the discussed in this paper features of CR cavity may be useful not only for the gravitational wave antennae but also in other high resolution spectroscopic experiments where the low level of optical eigenmode fluctuations is important.

Tilt of corner reflection

The tilt of one reflector through angle θ (see fig.C.3a) can be considered as displacement of lens on distance $\delta x \simeq l\,\theta$ (see fig.C.3b) perpendicular to axis. Then the set of integral equations (C.3, C.2) for eigen mode have the same form with replacing kernel $G_0 \to G_1$:

$$G_1 \simeq G_0 \left(1 - \frac{i x_1\,\delta x}{r_h^2}\right). \tag{C.41}$$

The perturbed main modes $\breve{\Phi}_1^{00}(x_1, y_1)$, $\breve{\Phi}_2^{00}(x_2, y_2)$ we find as expansion into series over eigen functions of resonator with perfectly positioned reflectors:

$$\breve{\Phi}_1^{00}(x_1, y_1) = \phi_0(y_1) \sum_m (-1)^m \alpha_m \phi_m(x_1)\,, \tag{C.42}$$

$$\breve{\Phi}_2^{00}(x_2, y_2) = \phi_0(y_2) \sum_m \beta_m \phi_m(x_2)\,. \tag{C.43}$$

After substitution these expansions into set (C.3, C.2) replacing kernel $G_0 \to G_1$ we obtain:

$$\begin{aligned} &\sum_m \lambda_m (-1)^m \alpha_m \phi_m(x_2) - \\ &\quad - e^{ikL} \int G_0(\vec{r}_1, \vec{r}_2) \left(\frac{i x_1\,\delta x}{r_h^2}\right) \times \\ &\qquad \times \sum_m (-1)^m \alpha_m \phi_m(x_1)\,dx_1 = \\ &= \Lambda \sum_m (-1)^m \beta_m \phi_m(x_2), \end{aligned} \tag{C.44}$$

$$\begin{aligned} &\sum_m \lambda_m \beta_m \phi_m(x_1) - e^{ikL} \int G_0(\vec{r}_1, \vec{r}_2) \times \\ &\qquad \times \left(\frac{i x_1\,\delta x}{r_h^2}\right) \sum_m \beta_m \phi_m(x_2)\,dx_2 = \\ &= \Lambda \sum_m \alpha_m \phi_m(x_1) \end{aligned} \tag{C.45}$$

Here Λ is eigen value of perturbed main mode.

After multiplying equation (C.44) by $\phi_{m_0}(x_2)$ and integrating we obtain:

$$\Lambda\,\beta_{m_0} = \lambda_{m_0,0}\alpha_{m_0} + I_{m_0}\,, \tag{C.46}$$
$$I_{m_0,0} = \frac{i\,\delta x\,r_L}{\sqrt{2}\,r_h^2}\,\lambda_{m_0,0}\times \times\left(\alpha_{m_0-1}\sqrt{m_0} + \alpha_{m_0+1}\sqrt{m_0+1}\right)$$

After multiplying equation (C.45) by $\phi_{m_0}(x_1)$ and integrating we obtain:

$$\Lambda\,m_0\alpha_{m_0} = \lambda_{m_0,0}\beta_{m_0} + J_{m_0,0}\,, \tag{C.47}$$
$$J_{m_0,0} = \frac{i\delta x\,r_L}{\sqrt{2}\,r_h^2}\left(\lambda_{m_0-1}\,\beta_{m_0-1}\,\sqrt{m_0} + \lambda_{m_0+1}\,\beta_{m_0+1}\,\sqrt{m_0+1}\right)$$

Now we can rewrite equations (C.46,C.47) for different m_0 taking in mind that $\alpha_0,\ \beta_0 \simeq 1$, $\alpha_1 \simeq\ \beta_1 = \mathcal{O}(\delta x)$, $\alpha_2 \simeq \beta_2 = \mathcal{O}(\delta x^2)$, $\ldots$:

$$m_0 = 0, \quad \lambda_0\,\alpha_0 + \frac{i\delta x\,r_L}{\sqrt{2}\,r_h^2}\,\lambda_0\alpha_1 = \Lambda\,\beta_0, \tag{C.48}$$
$$\Lambda\alpha_0 = \lambda_0\beta_0 + \frac{i\delta x\,r_L}{\sqrt{2}\,r_h^2}\,\lambda_1\beta_1, \tag{C.49}$$
$$\Rightarrow\alpha_0 \simeq \beta_0 \simeq 1, \quad \Lambda = \lambda_0 + \mathcal{O}(\delta x^2), \tag{C.50}$$

$$m_0 = 1, \quad \lambda_1\alpha_1 - \Lambda\beta_1 \simeq \frac{-i\delta x\,r_L}{\sqrt{2}\,r_h^2}\,\lambda_1\,, \tag{C.51}$$
$$-\Lambda\alpha_1 + \lambda_1\,\beta_1 \simeq \frac{-i\delta x\,r_L}{\sqrt{2}\,r_h^2}\,\lambda_0\,, \tag{C.52}$$
$$\Rightarrow\alpha_1 \simeq \frac{-i\delta x\,r_L\left(\lambda_1^2+\lambda_0^2\right)}{\sqrt{2}\,r_h^2\left(\lambda_1^2-\lambda_0^2\right)}, \tag{C.53}$$
$$\Rightarrow\beta_1 \simeq \frac{-i\delta x\,r_L\,\lambda_1}{\sqrt{2}\,r_h^2\left(\lambda_1-\lambda_0\right)}, \tag{C.54}$$

$$m_0 = 2, \quad \lambda_2\alpha_2 - \Lambda\beta_2 \simeq \frac{-i\delta x\,r_L}{\sqrt{2}\,r_h^2}\,\lambda_2\,\sqrt{2}\,\alpha_1, \tag{C.55}$$
$$-\Lambda\alpha_2 + \lambda_2\,\beta_2 \simeq \frac{-i\delta x\,r_L}{\sqrt{2}\,r_h^2}\,\sqrt{2}\,\lambda_1\,\beta_1, \tag{C.56}$$
$$\Rightarrow\alpha_2 \simeq \frac{-i\delta x\,r_L}{r_h^2}\frac{\left(\lambda_2^2\,\alpha_1 + \lambda_1\lambda_0\,\beta_1\right)}{\left(\lambda_2^2-\lambda_0^2\right)}, \tag{C.57}$$
$$\Rightarrow\beta_2 \simeq \frac{-i\delta x\,r_L}{r_h^2}\,\frac{\lambda_2\left(\lambda_0\,\alpha_1 + \lambda_1\,\beta_1\right)}{\left(\lambda_2^2-\lambda_0^2\right)}, \tag{C.58}$$

Rewriting values α_1 and β_1 using g-parameter (C.12 – C.14) one can obtain formulas (C.17 – C.19).

Displacement of CR

Let the right corner is displaced by value δx in transversal direction (see fig. C.4). Then the integral equations for perturbed eigen mode is the following

$$e^{ikL}\int G_1(x_1,y_1,x_2,y_2)\,\breve{\Phi}_1(x_1,y_1)\,dx_1\,dy_1 = \tag{C.59}$$

$$= \Lambda\,\breve{\Phi}_2(\delta x - x_2, -y_2), \tag{C.60}$$

$$e^{ikL}\int G_1(x_1,y_1,x_2,y_2)\,\breve{\Phi}_2(x_2,y_2)\,dx_2\,dy_2 = \tag{C.61}$$

$$= \Lambda\,\breve{\Phi}_1(-\delta x - x_1, -y_1), \tag{C.62}$$

$$\breve{\Phi}_1(-\delta x - x_1, -y_1) \simeq \breve{\Phi}_1(-x_1,-y_1) - \tag{C.63}$$

$$-\,\delta x\,\partial_{x_1}\breve{\Phi}_1(-x_1-y_1),$$

$$\breve{\Phi}_2(\delta x - x_2, -y_2) \simeq \breve{\Phi}_2(-x_2,-y_2) + \tag{C.64}$$

$$+\,\delta x\,\partial_{x_2}\breve{\Phi}_2(-x_2-y_2),$$

$$G_1(x_1,y_1,x_2,y_2) \simeq G_0(x_1,y_1,x_2,y_2)\times \tag{C.65}$$

$$\times\Big(1 - i\big[\delta h_1 + \delta h_2\big]\Big),$$

$$\delta h_1 \simeq \frac{x_1\delta x}{2r_h^2}, \quad \delta h_2 \simeq \frac{-x_2\delta x}{2r_h^2}. \tag{C.66}$$

We find perturbed main mode distributions $\breve{\Phi}_1^{00}(x_1,y_1)$, $\breve{\Phi}_2^{00}(x_2,y_2)$ as expansion into series over eigen functions of resonator with perfectly positioned reflectors:

$$\Phi_1^{00}(x_1,y_1) = \phi_0(y_1)\sum_m (-1)^m\alpha_m\phi_m(x_1) \tag{C.67}$$

$$\Phi_2^{00}(x_2,y_2) = \phi_0(y_2)\sum_m \beta_m\phi_m(x_2). \tag{C.68}$$

After substitution these expansions into (C.59 - C.65) we obtain:

$$\sum_m \lambda_{m,0}(-1)^m\alpha_m\phi_m(x_2) - e^{ikL}\int G_0(\vec{r}_1,\vec{r}_2)\times$$

$$\times\left(\frac{i(x_1-x_2)\delta x}{2r_h^2}\right)\sum_m(-1)^m\alpha_m\phi_m(x_1)\,dx_1 =$$

$$=\Lambda\sum_m(-1)^m\beta_m\phi_m(x_2) + \tag{C.69}$$

$$+\,\Lambda\,\delta x\sum_m(-1)^m\beta_m\left(\partial_{x_2}\phi_m(x_2)\right),$$

$$\sum_m \lambda_{m,0}\beta_m\phi_m(x_1) - e^{ikL}\int G_0(\vec{r}_1,\vec{r}_2)\times \tag{C.70}$$

$$\times\left(\frac{i(x_1-x_2)\delta x}{2r_h^2}\right)\sum_m\beta_m\phi_m(x_2)\,dx_2 =$$

$$=\Lambda\sum_m\alpha_m\phi_m(x_1) - \Lambda\,\delta x\sum_m\alpha_m\left(\partial_{x_1}\phi_m(x_1)\right),$$

After multiplying equation (C.69) by $\phi_{m_0}(x_2)$ and integrating we obtain:

$$\lambda_{m_0,0}\alpha_{m_0,0} + I_{m_0,0} = \Lambda\,\beta_{m_0,0} + J_{p_0,0}, \tag{C.71}$$
$$I_{m_0,0} = \frac{i\delta x\, r_l}{2\sqrt{2}\, r_h^2}\Big(\big[\lambda_{m_0,0} - \lambda_{m_0-1,0}\big]\sqrt{m_0}\alpha_{m_0-1} + \\ + \big[\lambda_{m_0,0} - \lambda_{m_0+1,0}\big]\sqrt{m_0+1}\alpha_{m_0+1}\Big),$$
$$J_{m_0,0} = -\frac{\Lambda\,\delta x}{r_L}\left(\beta_{m_0+1}\sqrt{\frac{m_0+1}{2}} - \beta_{m_0-1}\sqrt{\frac{m_0}{2}}\right).$$

After multiplying equation (C.70) by $\phi_{m_0}(x_1)$ and integrating we obtain:

$$\lambda_{m_0,0}\beta_{m_0,0} + I'_{m_0,0} = \Lambda\,\alpha_{m_0,0} + J'_{p_0,0}, \tag{C.72}$$
$$I'_{m_0,0} = \frac{i\delta x\, r_l}{2\sqrt{2}\, r_h^2}\big(\big[\lambda_{m_0,0} - \lambda_{m_0-1,0}\big]\sqrt{m_0}\alpha_{m_0-1} + \\ + \big[\lambda_{m_0,0} - \lambda_{m_0+1,0}\big]\sqrt{m_0+1}\alpha_{m_0+1}\big),$$
$$J'_{m_0,0} = \frac{-\Lambda\,\delta x}{\sqrt{2}\, r_L}\left(\alpha_{m_0+1}\sqrt{m_0+1} - \alpha_{m_0-1}\sqrt{m_0}\right).$$

Here we use the rule: coefficients $\alpha_m = 0$ and $\beta_m = 0$ if $m < 0$.

Substituting $I_{m_0,0}$ and $J_{m_0,0}$ into (C.71) and substituting $I'_{m_0,0}$ and $J'_{m_0,0}$ into (C.72) we obtain two equations. They may be transformed from one to other by replacement $\alpha_m \to \beta_m$ and vice versa $\beta_m \to \alpha_m$. So assuming that $\alpha_m = \beta_m$ we can solve only one equation:

$$\lambda_{m_0,0}\alpha_{m_0} + \frac{i\delta x\, r_L}{2\sqrt{2}\, r_h^2}\times \tag{C.73}$$
$$\times\Big(\big[\lambda_{m_0,0} - \lambda_{m_0-1,0}\big]\sqrt{m_0}\alpha_{m_0-1} + \\ + \big[\lambda_{m_0,0} - \lambda_{m_0+1,0}\big]\sqrt{m_0+1}\alpha_{m_0+1}\Big)$$
$$=\Lambda\,\alpha_{m_0} - \frac{\Lambda\,\delta x}{\sqrt{2}\, r_L}\left(\alpha_{m_0+1}\sqrt{m_0+1} - \alpha_{m_0-1}\sqrt{m_0}\right),$$

We assume that $\lambda_{0,0} = 1$, $\Lambda = \lambda_{0,0} + \Delta = 1 + \Delta$, $\alpha_0 \simeq 1$, $\alpha_1 \sim \delta x$, $\alpha_2 \sim \delta x^2$, ... Putting $m_0 = 0$ in (C.73) we obtain $\Delta \sim \delta x^2$. And putting $m_0 = 1$ in (C.73) we find

$$\alpha_1 \simeq -\alpha_0\,\frac{\delta x}{\sqrt{2}\, r_L}\left(\frac{i r_L^2}{2r_h^2} + \frac{1}{1-\lambda_{1,0}}\right) \tag{C.74}$$

Using (C.12 – C.14) one can rewrite this formula in form (C.20).

Table C.1: Numerical values of coefficients $F_{m_0,m}$ for low indices

	$m=0$	$m=2$	$m=4$	$m=6$
$m_0=0$	$1/\sqrt{\pi}$	$1/\sqrt{2\pi}$	$-1/(2\sqrt{6\pi})$	$1/(4\sqrt{5\pi})$

Expose perturbation of CR

For this case the equations for eigen modes calculations are the following in this section we do not mark by $\breve{}$ distribution function of perturbed mode:

$$e^{ikL}\int G_0(\vec{r}_1,\vec{r}_2)\,\Phi_2(\vec{r}_2)\,d\vec{r}_2 \simeq \tag{C.75}$$
$$\simeq \Lambda\tilde{\Phi}_1(\vec{r}_1)\Big(1-ib\gamma k|x_1|\Big),$$
$$e^{ikL}\int G_0(\vec{r}_1,\vec{r}_2)\,\Phi_1(\vec{r}_2)\,d\vec{r}_2 =\simeq \Lambda\tilde{\Phi}_2(\vec{r}_2).$$

We find the solutions as expansion

$$\Phi_1(x_1,y_1)=\phi_0(y_1)\sum_m(-1)^m\alpha_m\phi_m(x_1) \tag{C.76}$$
$$\Phi_2(x_2,y_2)=\phi_0(y_2)\sum_m\beta_m\phi_m(x_2). \tag{C.77}$$

Substituting them into equations (C.75, C.76) we obtain

$$\sum_m\lambda_{m,0}\beta_m\phi_m(x_1)= \tag{C.78}$$
$$=\Lambda\sum_m\alpha_m\phi_m(x_1)\Big(1-ib\gamma k|x_1|\Big),$$
$$\sum_m\lambda_{m,0}(-1)^m\alpha_m\phi_m(x_2)=\Lambda\sum_m(-1)^m\beta_m\phi_m(x_2) \tag{C.79}$$

From last equation we obtain

$$\beta_m=\frac{\lambda_{m,0}}{\Lambda}\,\alpha_m$$

and substitute it into (C.78). After multiplying obtained equation by $\phi_{m_0}(x_1)$ and integrating over dx_1 we get:

$$\lambda^2_{m,0}\alpha_{m_0}=\Lambda^2\,\alpha_{m_0}-ib\gamma\Lambda^2\,kr_L\sum_m\alpha_m\,F_{m_0,m}, \tag{C.80}$$

$$F_{m_0,m}=\int_{-\infty}^{\infty}|x|\,\phi_m(x)\,\phi_{m_0}(x)\,dx \tag{C.81}$$

We have tabulated coefficients F_{m,m_0} — result is presented in Table C.1.

Assuming that $\lambda_{0,0}=1$ and $\alpha_0\simeq 1,\ \alpha_1,\ \alpha_2,\cdots\ll 1$ we see that this system can be divided by two independent subsystems: one for odd indices and another one — for even

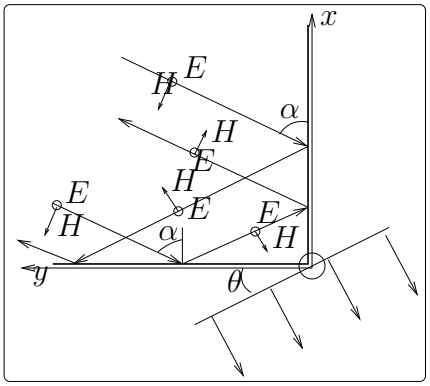

Figure C.6: Plane wave traveling and reflecting from dielectric corner reflector with angle between facets $\pi/2$. The axis z is directed upward and perpendicular to plane of figure. Vector E is directed along z-axis.

indices. Odd indices can be put zero and for even indices we have

$$\Lambda^2 \simeq 1 + \frac{iL\gamma r_L}{b\sqrt{\pi}}, \tag{C.82}$$

$$\alpha_2 \simeq \frac{iL\gamma k r_L}{\sqrt{2\pi}\, b\big(1 - e^{-8i\psi}\big)}, \tag{C.83}$$

$$\alpha_4 \simeq \frac{iL\gamma k r_L}{2\sqrt{6\pi}\, b\left(1 - e^{-16i\psi}\right)}, \tag{C.84}$$

We see that all coefficients $\alpha_2,\ \alpha_4, \cdots \sim \gamma$, i.e. they have the same order over γ. However the convergence seems to take place due to decreasing the coefficients $F_{m0,0} \sim 1/m_0^{5/4}$ with $m_0 \to \infty$.

These expressions can be rewritten using g-parameter in form (C.23, C.24).

Diffractional losses on edge

Here we write down the calculations to obtain estimate (C.36). We consider the monochromatic plane wave polarized along z-axis traveling and reflecting from dielectric CR with angle between facets $\pi/2$ (see fig. C.6). Incident wave:

$$E_{z\,\mathrm{inc}} = E_0 \exp\big(-i\omega t - ikn\sin\alpha\, x - ikn\cos\alpha\, y\big),$$
$$\vec{H} = \big[\vec{k}\,\vec{E}\big], \quad \mu = 1,$$

Below I drop the multiplier $e^{-i\omega t}$. Condition of internal reflection is fulfilled on both facets: $n\cos\alpha > 1, \qquad n\sin\alpha > 1$. We assume that magnetic permittivity $\mu = 1$ as in [23] and hence $n^2 = \epsilon$ (ϵ dielectric permittivity).

Field inside CR. We use Fresnel formulas for light wave reflection from plane boundary between dielectric and vacuum using complex reflection coefficient $R_\perp$ [23] (for the case of complete internal reflection):

$$R_\perp(\beta) = \frac{ncos\beta - i\sqrt{n^2 sin^2\beta - 1}}{ncos\beta + i\sqrt{n^2 sin^2\beta - 1}}$$

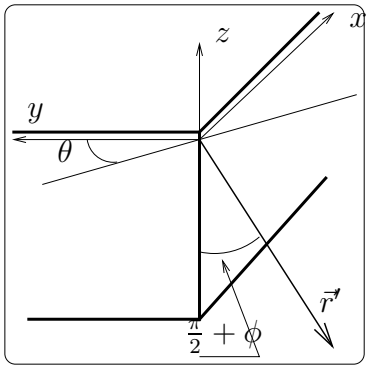

Figure C.7:

where β is incident angle. The sum field after two reflections from both facets *inside* dielectric is the following:

$$E_z = E_0 \Big(e^{-ik_x x - ik_y y} + R_\perp(\alpha) e^{+ik_x x - ik_y y} + \tag{C.85}$$
$$+ R_\perp(\pi/2-\alpha) e^{-ik_x x + ik_y y} +$$
$$+ \; R_\perp(\pi/2-\alpha) R_\perp(\alpha) e^{+ik_x x + ik_y y} \Big),$$
$$k = \frac{\omega}{c}, \quad k_x = kn\cos\alpha, \quad k_y = kn\sin\alpha \tag{C.86}$$

The first terms in brackets describe the incident wave, the second and third terms — the waves reflected from planes $(y = 0)$ and $(x = 0)$ correspondingly, the last term describes wave double reflected from both planes.

We simplify formula (C.85) and calculate magnetic field:

$$E_z = 4E_0 e^{-i(\delta_x+\delta_y)} \cos(k_x x - \delta_x)\, \cos(k_y y - \delta_y), \tag{C.87}$$
$$\tan\delta_x = \frac{\sqrt{n^2\sin^2\alpha - 1}}{n\cos\alpha}, \quad \tan\delta_y = \frac{\sqrt{n^2\cos^2\alpha - 1}}{n\sin\alpha} \tag{C.88}$$

The field on outside surface of CR Now we can write down the expressions for fields outside CR in planes $x = 0 - \epsilon,\ y = 0 - \epsilon$ using boundary conditions — continuity of tangent component of $\vec{E}$ and normal component $\mu\vec{H}$. Then the expressions for fields are the following:

$$E_z^{x=0} = 4E_0 e^{-i(\delta_x+\delta_y)} \cos(\delta_x)\, \cos(k_y y - \delta_y),$$
$$H_x^{x=0} = 4i\, nE_0 \sin\alpha\, e^{-i(\delta_x+\delta_y)} \cos(\delta_x)\, \sin(k_y y - \delta_y),$$
$$H_y^{x=0} = i4nE_0\, \cos\alpha\, e^{-i(\delta_x+\delta_y)} \sin(\delta_x)\, \cos(k_y y - \delta_y),$$
$$E_z^{y=0} = 4E_0 e^{-i(\delta_x+\delta_y)} \cos(k_x x - \delta_x)\, \cos(\delta_y),$$
$$H_x^{y=0} = -4inE_0\, \sin\alpha\, e^{-i(\delta_x+\delta_y)} \cos(k_x x - \delta_x)\, \sin(\delta_y),$$
$$H_y^{y=0} = -4inE_0\, \cos\alpha\, e^{-i(\delta_x+\delta_y)} \sin(k_x x - \delta_x)\, \cos(\delta_y)$$

We take in mind that plane wave is limited by Gaussian multiplier

$$b = \exp\Big(- a^2 \big([x\sin\alpha - y\cos\alpha]^2 + z^2 \big) \Big)$$

with small parameter a, or more precisely: $a \ll k$.

Radiation field. We can apply diffraction Green formula to E_z and calculate it in far wave zone in direction characterized by angles $\phi,\ \theta$ and distance $|\vec{r} - \vec{r}'|$ (see fig.C.7):

$$E_z(\vec{r}') = \int \Big(E_z \partial_n G(R) - \ G(R) \partial_n E_z \Big)\, d\vec{r}, \tag{C.89}$$

$$G(R) = \frac{e^{ikR}}{4\pi\, R}, \quad R = |\vec{r}' - \vec{r}| \gg \frac{1}{k}, \tag{C.90}$$

$$\partial_n G(R) \simeq -ikG(R) \times \frac{\vec{n}(\vec{r}' - \vec{r})}{R}. \tag{C.91}$$

Here $\vec{r}'$ is radius-vector of observation point, $\vec{r}$ is radius-vector of point on surface of integration, $d\vec{r}$ is element of integration surface, $\vec{n}$ is normal to surface of integration. The result of calculations is the following:

$$E_z(R) = \frac{iE_0\, e^{ikr'}\, e^{-i(\delta_x + \delta_y)}}{\pi R} \times \tag{C.92}$$

$$\times \underbrace{\frac{\sqrt{\pi}\, e^{-k^2 \sin^2\phi/4a^2}}{a}}_{f(k\phi) \to \delta(k\phi)} \times \Big(I_x + I_y \Big),$$

$$I_x = kb_x \int_0^\infty dx\ \cos(k_x x - \delta_x) e^{ikx cos\theta}\, e^{-a^2 x^2 \sin^2\alpha} \simeq$$

$$\simeq \frac{b_x \big(n \cos\alpha\ \sin\delta_x - i \cos\theta\ \cos\delta_x \big)}{n^2 \cos^2\alpha - \cos^2\theta}, \tag{C.93}$$

$$I_y = kb_y \int_0^\infty dy\ \cos(k_y y - \delta_y)\, e^{iky \sin\theta}\, e^{-a^2 y^2 \cos^2\alpha} \simeq$$

$$\simeq \frac{b_y \big(n \sin\alpha\ \sin\delta_y - i \sin\theta\ \cos\delta_y \big)}{n^2 \sin^2\alpha - \sin^2\theta} \tag{C.94}$$

Above we used auxiliary formulas:

$$I_c(k) = \int_0^\infty \cos kx\, e^{-a^2 x^2}\, dx \ \Rightarrow\ \pi\, \delta(k), \quad \text{if } a \ll k, \tag{C.95}$$

$$I_s(k) = \int_0^\infty \sin kx\, e^{-a^2 x^2}\, dx \ \Rightarrow\ \frac{1}{k}, \quad \text{if } a \ll k,$$

Power of diffraction losses W can be calculated as following

$$W = \int_{-\pi/2}^{\pi/2} \int_{-\pi/2}^{\pi} \frac{|E_z|^2 c}{2\pi}\, R^2\, \cos\phi\, d\phi\, d\theta = \frac{E_0^2 c}{2\pi^3} \times \frac{2\sqrt{\pi}}{ka} \times A,$$

$$A = \int_{-\pi/2}^{\pi} \big(I_x + I_y \big)^2\, d\theta \tag{C.96}$$

We have to compare the value W with total power W_0 of incident wave

$$W_0 = \frac{E_0^2 c}{2a^2}, \qquad (1 - R)_d = \frac{W}{W_0} = \frac{2a}{\pi^2 \sqrt{\pi}\, k} \times A, \tag{C.97}$$

Replacing notations $a \to 1/\sqrt{2}\, R_b$ and calculating numerically integral $A \simeq 32.8$ for $n = 1.45$ ($Si\, O_2$) and $\alpha = \pi/4$ we finally obtain the estimate (C.36).

TD temperature fluctuations in thermo-isolated layer

We have thermal conductivity equation for temperature $u(\vec{r},t)$ in infinite layer with width l ($0 \le z \le l$) with fluctuating force in right part [9] and the following boundary conditions:

$$\frac{\partial u}{\partial t} - a^2 \Delta u = F(\vec{r},t), \tag{C.98}$$

$$\left.\frac{\partial u(\vec{r},t)}{\partial z}\right|_{z=0,\,l} = 0, \tag{C.99}$$

$$\langle\, F(\vec{r},t) F(\vec{r}',t') \,\rangle = -\frac{2\kappa\, k_B T^2}{(\rho C)^2}\, \Delta\delta(\vec{r}-\vec{r}')\, \delta(t-t'), \tag{C.100}$$

where $a^2 = \kappa/\rho C$, k_B is Boltzmann constant, δ is Dirac delta function.

We find solution as series:

$$\begin{aligned}
u(\vec{r},t) &= \iiint_{-\infty}^{\infty} \frac{dk_x dk_y d\omega}{(2\pi)^3} \sum_n u_n(k_x,k_y,\omega) \times \\
&\quad \times e^{i\omega t - ik_x x - ik_y y}\, \cos b_n z, \\
u_n(k_x,k_y,\omega) &= \frac{F_n(k_x,k_y,\omega)}{i\omega + a^2(b_n^2 + k_\perp^2)}, \\
b_n &= \frac{\pi n}{l}, \quad k_\perp^2 = k_x^2 + k_y^2, \\
u_n(k_x,k_y,\omega) &= \iiint_{-\infty}^{\infty} dx\, dy\, dt\, e^{-i\omega t + ik_x x + ik_y y} \times \\
&\quad \times \int_0^l dz\, \frac{2-\delta_{0,n}}{l}\, \cos b_n z\, u(x,y,z,t),
\end{aligned}$$

We find correlation functions of coefficients $F_n(k_x,k_y,\omega)$:

$$\begin{aligned}
F_{n,n_1} &= \langle\, F_n(k_x,k_y,\omega) F_{n_1}^*(k_{x_1},k_{y_1},\omega_1) \,\rangle = \\
&= \frac{2(2\pi)^3 k_B T^2 \kappa}{(\rho C)^2} \left(k_\perp^2 + b_n^2\right) \frac{2-\delta_{0,n}}{l}\, \delta_{n,n_1} \times \\
&\quad \times \delta(k_x - k_{x_1})\, \delta(k_y - k_{y_1})\, \delta(\omega - \omega_1).
\end{aligned}$$

We are interested in temperature $\bar{u}(t,x_0,y_0)$, averaged over volume $V = \pi R_b^2 l$ along axis parallel to axis z with transversal coordinates x_0 and y_0, and also its correlation

function $\langle\, \bar{u}(t,0,0)\bar{u}(t+\tau), x_0, y_0\,\rangle$ with spectral density $S_{\bar{u}}(\omega)$:

$$\begin{aligned}
\bar{u}(t,x_0,y_0) &= \frac{1}{\pi R_b^2 l}\int_0^l dz \iint_{-\infty}^{\infty} dx\, dy \times \\
&\times u(\vec{r},t) e^{-\frac{(x-x_0)^2+(y-y_0)^2}{R_b^2}} = \\
&= \int_0^l \frac{dz}{l} \iint_0^{\infty} \frac{dx\, dy}{\pi R_b^2} e^{-\frac{(x-x_0)^2+(y-y_0)^2}{R_b^2}} \times \\
&\times \iiint_{-\infty}^{\infty} \frac{dk_x dk_y d\omega}{(2\pi)^3} \sum_n u_n(k_x,k_y,\omega) \times \\
&\times \cos b_n z\, e^{i\omega t - ik_x x - ik_y y} = \\
&= \iiint_{-\infty}^{\infty} \frac{dk_x dk_y d\omega}{(2\pi)^3} e^{-\frac{R_b^2 k_\perp^2}{4}} \times \\
&\times e^{i\omega t - ik_x x_0 - ik_y y_0}\, u_0(k_x,k_y,\omega),
\end{aligned} \tag{C.101}$$

$$\begin{aligned}
B_{\bar{u}}(\tau) &= \langle\, \bar{u}(t,0,0)\bar{u}(t+\tau,x_0,y_0)\,\rangle = \\
&= \frac{2k_B T^2 \kappa}{(\rho C)^2} \frac{1}{l} \iiint_{-\infty}^{\infty} \frac{dk_x dk_y d\omega}{(2\pi)^3} \times \\
&\times e^{-\frac{R_b^2 k_\perp^2}{2} - ik_x x_0 - ik_y y_0} \frac{k_\perp^2 e^{i\omega\tau}}{\omega^2 + a^4 k_\perp^4} = \\
&= \frac{k_B T^2}{(\rho C)} \frac{1}{\pi R_b^2 l (1 + 2a^2\tau/R_b^2)} e^{-\frac{x_0^2+y_0^2}{2(R_b^2+2a^2\tau)}},
\end{aligned} \tag{C.102}$$

$$\begin{aligned}
S_{\bar{u}}(\omega) &= 2\int_{-\infty}^{\infty} d\tau\, e^{i\omega\tau} \langle\, \bar{u}(t,0,0)\bar{u}(t+\tau,0,0)\,\rangle = \\
&= \frac{4k_B T^2 \kappa}{(\rho C)^2 l} \int_0^{\infty} \frac{k_\perp dk_\perp}{2\pi} e^{-\frac{R_b^2 k_\perp^2}{2}} \frac{k_\perp^2}{\omega^2 + a^4 k_\perp^4}
\end{aligned} \tag{C.103}$$

Making following substitutions

$$\xi = \frac{k_\perp^2 R_b^2}{2}, \quad w = \frac{\omega R_b^2}{2\,a^2}, \quad a^2 = \frac{\kappa}{\rho C} \tag{C.104}$$

one can express the spectral density using exponential integrals:

$$\begin{aligned}
S_{\bar{u}}(\omega) &= \frac{k_B T^2}{\pi \rho C l\, a^2} \int_0^{\infty} \frac{\xi\, d\xi}{w^2 + \xi^2} e^{-\xi} = \\
&= \frac{k_B T^2}{2\pi \rho C l\, a^2} \times \\
&\times \Big(e^{iw} \mathrm{Ei}_1(iw) + e^{-iw} \mathrm{Ei}_1(-iw) \Big), \\
\mathrm{Ei}_n(x) &= \int_1^{\infty} e^{-x\,t} \frac{dt}{t^n}
\end{aligned}$$

For particular cases this formula can be simplified:

$$S_{\bar{u}}(\omega)|_{w\ll 1} \simeq \frac{4k_B T^2 \kappa}{(\rho C)^2 l} \frac{1}{\pi R_b^4 \omega^2}, \tag{C.105}$$

$$S_{\bar{u}}(\omega)|_{w\gg 1} \simeq \frac{4k_B T^2}{\rho C \pi R_b^2 l} \times \frac{r_T^2}{R_b^2 \omega}. \tag{C.106}$$

The formulas (C.105 and C.106) refer to non-adiabatic and adiabatic cases correspondingly.

Parameters

For our estimates we used the following parameters, material parameters correspond to fused silica.

$$\begin{aligned}
&\omega = 2\pi \times 100 \text{ s}^{-1}, \quad \lambda = 1.064 \ \mu\text{m}, \quad T = 300 \text{ K}, \\
&b = 2.3 \text{ cm}, \quad R_b \simeq 6 \text{ cm} \\
&m = 4 \times 10^4 \text{ g}, \quad L = 4 \times 10^5 \text{ cm}; \\
&\alpha = 5.5 \times 10^{-7} \text{ K}^{-1}, \quad \kappa = 1.4 \times 10^5 \ \frac{\text{erg}}{\text{cm s K}}, \\
&\rho = 2.2 \ \frac{\text{g}}{\text{cm}^3}, \quad C = 6.7 \times 10^6 \ \frac{\text{erg}}{\text{g K}}, \\
&n = 1.45, \quad \beta = \frac{dn}{dT} = 1.5 \cdot 10^{-5} \text{ K}^{-1}
\end{aligned}$$

References

[1] J. Ye, D. E. Vernooy and H. J. Kimble, "Trapping of single atoms in cavity QED", quant-ph/9908007.

[2] H. J. Kimble, private communication.

[3] G. Rempe et al, *Opt.Letters*, **17**, 363 (1992).

[4] A. Abramovici et al, *Science* **256**, 326 (1992).

[5] A. Abramovici et al, *Phys.Letters.* **A218**, 157 (1996).

[6] V. B. Braginsky and F. Ya. Khalili, *Quantum Measurement*, ed. by K.S. Thorne, Cambridge Univ. Press, 1992.

[7] V. B. Braginsky and F. Ya. Khalili, *Rev. Mod. Physics*, **68**, 1 (1996).

[8] F. Ya. Khalili, *Physics Letters* **A317**, 169 (2003)

[9] V. B. Braginsky, M. L. Gorodetsky, and S. P. Vyatchanin, *Physics Letters* **A 264**, 1 (1999); cond-mat/9912139;

[10] V. B. Braginsky and S. P. Vyatchanin, *Physics Letters* **A312**, 244 (2003); arXiv: cond-mat/0302617,

[11] G. Cagnoli, D. Crooks, M. M. Fejer, Gregg Harry, Jim Hough, Norio Nakagawa, Steve Penn, Roger Route, Sheila Rowan, P. Sneddon, LIGO document: G030195-00, (2003)

[12] M. M. Fejer, S.Rowan, D. Crooks, P. Sheddon, G. Harry, J. Hough, S. Penn, to be published in *Phys.Rev.D.*

[13] V.B.Braginsky, A.A. Samoilenko, *Physics letters* **A315**, 175 (2003), arXiv:gr-qc/0304100v1.

[14] V. B. Braginsky, M. L. Gorodetsky, F. Ya. Khalili and K. S. Thorne, *Report at Third Amaldi Conference, Caltech*, July, 1999.

[15] Benvenuto Cellini, Autobiography, Penguin Books Ltd, 1956.

[16] Izwin I. Shapiro et al, Phys. Rev. Lett. **36**, 555 (1976); J. G. Williams et al, Phys. Rev. Lett. **36**, 551 (1976).

[17] V. B. Braginsky, M. L. Gorodetsky, and S. P. Vyatchanin, *Physics Letters* **A 271**, 303-307 (2000)

[18] A. E. Siegman, Lasers, Univ. Science Book, 1996, ch. 19

[19] LIGO-II conceptual project book. LIGO document M990288-A1, available on www.ligo.caltech edu.

[20] E. d'Ambrosio, R. O'Shaughnessy, S. Strigin, K.Thorne and S. Vyatchanin, Reducing Thermoelastic Noise in Gravitational-Wave Interferometers by Flattening the Light Beams, submitted to *Phys. Rev. D*,
available as file beamreshape020903.pdf at http://www.cco.caltech.edu/∼kip/ftp/

[21] O'Shaughnessy, S. Strigin and S. Vyatchanin, The implifications of Mexican-hat mirrors: calculations of thetmoelastic noise and interferometer sensitivity to perturbation for Mexican-hat mirror proposal for advanced LIGO, submitted to *Phys. Rev. D*.

[22] Garrilynn Billingsley, private communication.

[23] L. D. Landau and E. M. Lifshitz, Electrodinamics of continious media, Moscow, 1982. sec. 86.

[24] D.R.Crooks, P.Sneddon, G.Gagnoli, J.Hough, S.Rowan, M.M.Fejer, E.Gustavson, R.Route, N.Nakagawa, G.M.Harry, A.M.Gretarsson, to be published in *Classical and Quantum Gravity*.

[25] D.R.Crooks et al, *Classic and Quantum Gravity*, **19**, 4229, (2002).

[26] G. Harry et al, et al, *Classic and Quantum Gravity*, **19**, 897, (2002).

[27] S. Penn et al, *Classic and Quantum Gravity*, **20**, 2917, (2003).

[28] N. Nakagawa et al, Phys. Rev. D, **65**, 102001, (2002).

[29] Numata eat al *Phys.Rev.Lett.* **91**, 260602 (2202).

[30] E. Black et al, submitted to *Phys.Rev.Lett.*

Appendix D

Reducing the mirrors coating noise in laser gravitational-wave antennae by means of double mirrors

Recent researches show that the fluctuations of the dielectric mirrors coating thickness can introduce a substantial part of the future laser gravitational-wave antennae total noise budget. These fluctuations are especially large in the high-reflectivity end mirrors of the Fabry-Perot cavities which are being used in the laser gravitational-wave antennae.

We show here that the influence of these fluctuations can be substantially decreased by using additional short Fabry-Perot cavities, tuned in anti-resonance instead of the end mirrors.

Introduction

One of the basis components of laser gravitational-wave antennae [1, 2, 3] are high-reflectivity mirrors with multilayer dielectric coating. Recent researches [4, 5, 6, 7, 8, 9, 10, 11, 12, 13] have shown that fluctuations of the coating thickness produced by, in particular, Brownian and thermoelastic noise in a coating, can introduce substantial part of the total noise budget of the future laser gravitational-wave antennae. For example, estimates, done in [9] show that the thermoelastic noise value can be close to the Standard Quantum Limit (SQL) [14] which corresponds to the sensitivity level of the Advanced LIGO project [3] or even can exceed it in some frequency range.

For this reason it was proposed in [15] to replace end mirrors by coatingless corner reflectors. It was shown in this article that by using these reflectors, it is possible, in principle, to obtain sensitivity much better than the SQL. However, the corner reflectors require substantial redesign of the gravitational-wave antennae core optics and suspension system.

At the same time, the value of the mirror surface fluctuations depends on the number of dielectric layers which form the coating. It can be explained in the following way. The most of the light is reflected from the first couple of the layers. At the same time, fluctuations of the mirror surface are created by the thickness fluctuations of all underlying layers, and the larger is the layers number, the larger is the surface noise.

Therefore, the surface fluctuations are relatively small for the input mirrors (ITM) of the Fabry-Perot cavities of the laser gravitational-wave antennae with only a few coating layers and $1 - \mathcal{R} \sim 10^{-2}$ ($\mathcal{R}$ is the mirror power reflectivity), and is considerably larger

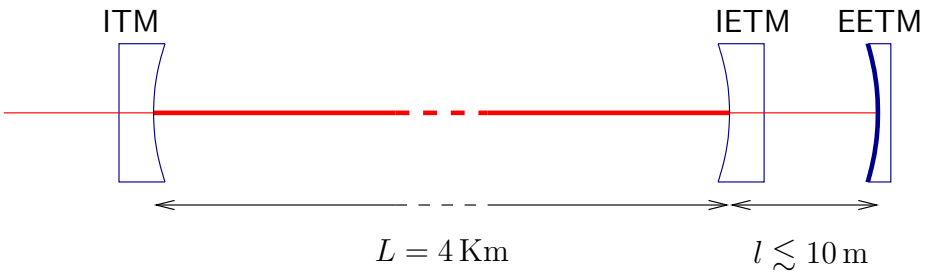

Figure D.1: Schematic layout of a Fabry-Perot cavity with double mirror system instead of the end mirror: ITM and IETM are similar moderate reflective mirrors; EETM is a high-reflective one.

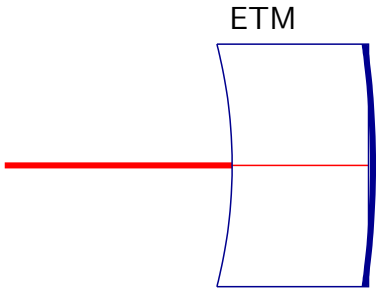

Figure D.2: The double reflector based on a single mirror.

for the end mirrors (ETM) with coating layers number ~ 40 and $1 - \mathcal{R} \lesssim 10^{-5}$.

In this paper another, less radical way of reducing the coating noise, exploiting this feature, is proposed. It is based on the use of an additional short Fabry-Perot cavity instead of the end mirror (see Fig. D.1). It should be tuned in anti-resonance, *i.e* its optical length l should be close to $l = (N + 1/4)\lambda$, where λ is a wavelength. The back side of the first mirror have to have a few layers of an antireflection coating.

It can be shown that in this case reflectivity of this cavity will be defined by the following equation:

$$1 - \mathcal{R} \approx \frac{(1 - \mathcal{R}_1)(1 - \mathcal{R}_2)}{4}\,, \tag{D.1}$$

where $\mathcal{R}_{1,2}$ are the reflectivities of the first (EETM on Fig. D.1) and the second (IETM) mirrors. Phase shift in the reflected beam produced by small variations y in position of the second mirror reflecting surface relative to the first one will be equal to

$$\phi \approx \frac{1 - \mathcal{R}_1}{4} \times 2ky\,, \tag{D.2}$$

where $k = 2\pi/\lambda$ is a wave number. It is supposed for simplicity that there is no absorption in the first mirror material; more general formulae are presented below.

It follows from these formulae that the first mirror can have a moderate value of reflectivity and, therefore, a small number of coating layers. In particular, it can be identical to the input mirror of the main Fabry-Perot cavity (ITM). At the same time, influence of the coating noise of the second (very-high-reflective) mirror will be suppressed by a factor of $(1 - \mathcal{R}_1)/4$, which can be as small as $\sim 10^{-2} \div 10^{-3}$.

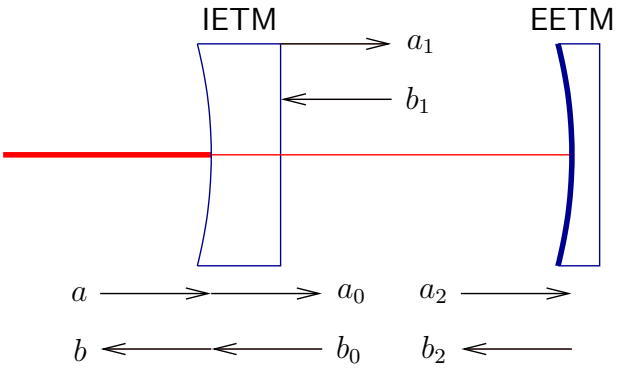

Figure D.3: The double mirror reflector.

In principle, another design of the double reflector is possible, which consists of one mirror only, see Fig. D.2. Both surfaces of this mirror have to have reflective coatings: the thin one on the face side and the thick one on the back side. In this case the additional Fabry-Perot cavity is created *inside* this mirror. However, in this case thermoelastic fluctuations of the the back surface coating will bend the mirror and thus will create unacceptable large mechanical fluctuations of the face surface. Estimates show that using this design, it possible to reduce the face surface fluctuations by factor ~ 3 only [16]. So the design with two *mechanically isolated* reflectors only will be considered here.

In the next section more detail analysis of this system is presented.

Analysis of the double-mirror reflector

The rightmost part of Fig. D.1 is presented in Fig. D.3, where the following notation is used:

a, b are the amplitudes of the incident and reflected waves for the first mirror, respectively;

a_0, b_0 are the amplitudes of the waves traveling in the left and right directions, respectively, just behind the first mirror coating;

a_1, b_1 are the same for the waves just behind the first mirror itself;

a_2, b_2 are the amplitudes of the incident and reflected waves for the second mirror, respectively.

These amplitudes satisfy the following equations:

$$a_0 = -R_1 b_0 + iT_1 a\,, \tag{D.3a}$$
$$a_1 = T_0 a_0 + A_1 n_a\,, \tag{D.3b}$$
$$a_2 = \theta a_1\,, \tag{D.3c}$$
$$b = -R_1 a + iT_1 b_0\,, \tag{D.3d}$$
$$b_0 = T_0 b_1 + A_0 n_b\,, \tag{D.3e}$$
$$b_1 = \theta b_2\,, \tag{D.3f}$$
$$b_2 = -R_2 a_2 + A_2 n_2\,, \tag{D.3g}$$

where:

n_a, n_b, n_2 are independent zero-point oscillations generated in the first (n_a, n_b) and the second (n_2) mirrors;

$\theta = e^{ikl_1}$, where l_1 is the distance between the first mirror back surface and the second mirror;

$-R_1$ and iT_1 are the amplitude reflectivity and transmittance of the first mirror coating, respectively, $R_1^2 + T_1^2 = 1$;

T_0 and A_0 are the amplitude transmittance and absorption of the first mirror bulk, respectively, $|T_0|^2 + A_0^2 = 1$;

$-R_2$ and A_2 are the amplitude reflectivity and absorption of the second mirror, respectively, $R_2^2 + A_2^2 = 1$.

R_1, T_1, A_0, R_2, A_2 are real values; T_0 is a complex one, its argument corresponds to the phase shift in the first mirror bulk.

Here we do not consider absorption in the first mirror coating for two reasons: (i) it is relatively small and (ii) it exists both in traditional one-mirror reflectors and in the one considered here, and the main goal of this short article is to emphasize the *differences* between these two types of reflectors.

It follows from equations (D.3) that the reflected beam amplitude is equal to

$$b = \frac{(R_2 T_0^2 \theta^2 - R_1)a - iR_2 A_0 T_0 T_1 \theta^2 n_a + iA_2 T_0 T_1 \theta n_2 + iA_0 T_1 n_b}{1 - R_1 R_2 T_0^2 \theta^2}\,. \tag{D.4}$$

This solution can be presented in the following form:

$$b = \tilde{R}a + An\,, \tag{D.5}$$

where

$$\tilde{R} = \frac{R_2 T_0^2 \theta^2 - R_1}{1 - R_1 R_2 T_0^2 \theta^2} \tag{D.6}$$

is the equivalent complex reflection factor for the scheme considered,

$$A = \frac{T_1 \sqrt{1 - R_2^2 |T_0|^4}}{|1 - R_1 R_2 T_0^2 \theta^2|} \tag{D.7}$$

is its equivalent absorption factor, and

$$n = \frac{1}{A}\,\frac{-iR_2 A_0 T_0 T_1 \theta^2 n_a + iA_2 T_0 T_1 \theta n_2 + iA_0 T_1 n_b}{1 - R_1 R_2 T_0^2 \theta^2} \tag{D.8}$$

is the sum noise normalized as zero-point fluctuations.

As mentioned above, this system should be tuned in anti-resonance:

$$l \equiv \frac{1}{k} \arg T_0 \theta = \frac{\pi}{k}\left(N + \frac{1}{2}\right) + y\,, \tag{D.9}$$

where N is an integer and $y \ll \lambda$. In this case

$$T_0 \theta = i(-1)^N |T_0| e^{iky} \approx i(-1)^N (1 + iky)\,, \tag{D.10}$$

and

$$\tilde{R} \approx -Re^{i\phi}\,, \tag{D.11}$$

where

$$R = 1 - \frac{(1-R_1)(1-R_2|T_0|^2)}{1+R_1R_2|T_0|^2}\,, \tag{D.12}$$

and

$$\phi \approx \frac{2R_2|T_0|^2T_1^2}{(R_2|T_0|^2+R_1)(1+R_1R_2|T_0|^2)}\,ky \tag{D.13}$$

is the phase shift produced by the deviation y in the distance l.

Suppose that factors T_1, A_0, A_2 are small. In this case

$$1 - R \approx \frac{(1-R_1)(1-R_2+A_0^2)}{2}\,, \tag{D.14}$$

$$\phi \approx (1-R_1)ky\,. \tag{D.15}$$

Using power reflection and absorption factors instead of the amplitude ones:

$$\mathcal{R} = R^2\,, \tag{D.16}$$

$$\mathcal{R}_{1,2} = R_{1,2}^2\,, \tag{D.17}$$

$$\mathcal{A}_0 = A_0^2\,, \tag{D.18}$$

equations (D.14), (D.15) can be rewritten as follows:

$$1 - \mathcal{R} \approx \frac{(1-\mathcal{R}_1)(1-\mathcal{R}_2+2\mathcal{A}_0)}{4}\,, \tag{D.19}$$

$$\phi \approx \frac{1-\mathcal{R}_1}{2}\,ky\,. \tag{D.20}$$

Conclusion

The main goal of this short article is just to claim the idea, so the detailed design of the additional cavity is not presented here. However, the following important topics have to be discussed in brief.

The first one concerns the optimal value of the IETM mirror reflectivity. The smaller is $1-\mathcal{R}_1$, the larger is suppression factor for the EETM mirror surface noises; at the same time, the larger is the IETM mirror coating noise. The rigorous optimization requires exact knowledge of the coating noise dependence on the coating layers number.

A crude estimate based in the exponential dependence of the IETM mirror transmittance $\mathcal{T}_1 \approx 1-\mathcal{R}_1$ on the coating layers number gives that the optimal transmittance value is relatively large, $\mathcal{T}_1 \sim 10^{-1}$. On the other hand, smaller values of the IETM mirror transmittance, down to the input (ITM) mirror transmittance $\mathcal{T}_{\mathsf{ITM}}$ are also acceptable. Therefore, identical ITM and IETM mirrors can be used.

In the Advanced LIGO interferometer, the input mirrors transmittance will be equal to $\mathcal{T}_{\mathsf{ITM}} \approx 5\times10^{-3}$, and its bulk absorption will be equal to $\mathcal{A}_{\mathrm{ITM}} \approx 10^{-5}$ [17]. Using such mirror as an IETM mirror in the scheme proposed in this article, and mirror with commercially available value of $1-\mathcal{R}_2 \approx 10^{-5}$ as an EETM mirror, it is possible to create

a double-mirror reflector with $1-\mathcal{R} < 10^{-6}$ and suppression factor for the EETM surface fluctuations $\dfrac{1-\mathcal{R}_1}{4} \approx 10^{-3}$.

The second issue concerns the optical power circulating through the IETM mirror. It is easy to show using equations (D.3), that it is $\dfrac{4}{1-\mathcal{R}_1} \sim 10^3$ times smaller that the power circulating in the main cavities. In the Advanced LIGO topology, it will be approximately equal to the power circulating through the ITM mirrors and the beamsplitter (about 1 KW).

It is necessary to note also that y in the calculations presented above includes not only coating noise of the EETM mirror but all possible kinds of its surface fluctuations, including ones caused by Brownian and thermoelastic fluctuations in this mirror bulk, Brownian fluctuation in its suspension, seismic noise as well as the mirror quantum fluctuations. This feature simplifies greatly the EETM mirror design because the requirements for all these noise sources can be reduced by a factor of $(1-\mathcal{R}_1)/4$.

In particular, the SQL value $\sqrt{\dfrac{\hbar}{m\Omega^2}}$ for this mirror (m is its mass and Ω is the observation frequency) can be larger by a factor of $\left(\dfrac{1-\mathcal{R}_1}{4}\right)^{-1}$. Therefore, its mass can be, in principle, $\left(\dfrac{1-\mathcal{R}_1}{4}\right)^{-2} \sim 10^6$ times smaller than for the main (ITM and IETM) mirrors. Of course, such a small mirror hardly can be used in the real interferometer. This estimates shows only that the quantum noise does not impose any practical limitation on the EETM mirror mass.

References

[1] A.Abramovici *et al*, Science **256**, 325 (1992).

[2] A.Abramovici *et al*, Physics Letters A **218**, 157 (1996).

[3] E.Gustafson, D.Shoemaker, K.A.Strain and R.Weiss, LSC White paper on detector research and development, 1999, LIGO Document T990080-00-D (www.ligo.caltech.edu/docs/T/T990080-00.pdf).

[4] Yu.Levin, Physical Review D **57**, 659 (1998).

[5] D.Crooks *et al*, Classical and Quantum Gravity **19**, 883 (2002).

[6] G.M.Harry *et al*, Classical and Quantum Gravity **19**, 897 (2002).

[7] N.Nakagawa, A.M.Gretarsson, E.K.Gustafson and M.M.Fejer, Physical Review D **65**, 102001 (2002).

[8] S.D.Penn *et al*, Classical and Quantum Gravity **20**, 2917 (2003).

[9] V.B.Braginsky, S.P.Vyatchanin, Physics Letters A **312**, 169 (2003).

[10] V.B.Braginsky, A.A. Samoilenko, Physics Letters A **315**, 175 (2003).

[11] G.Cagnoli *et al*, LIGO Document G0301195-00 (2003).

[12] M.M.Fejer *et al*, arXiv:gr-qc/0402034 (2004).

[13] G.M.Harry *et al*, LIGO Document P040023-00 (2004).

[14] V.B.Braginsky *et al*, Physical Review D **67**, 082001 (2003).

[15] V.B.Braginsky, S.P.Vyatchanin, arXive:cond-mat/0402650 (2004).

[16] S.P.Vyatchanin, *private communication.*

[17] www.ligo.caltech.edu/AdvLIGO